

Interesting Clues to Detect Hidden Tidal Disruption Events in Active Galactic Nuclei

Xue-Guang Zhang^{*}

Guangxi Key Laboratory for Relativistic Astrophysics, School of Physical Science and Technology, Guangxi University, Nanning, 530004, P. R. China

ABSTRACT

In the manuscript, effects of Tidal Disruption Events (TDEs) are estimated on long-term AGN variability, to provide interesting clues to detect probable hidden TDEs in normal broad line AGN with apparent intrinsic variability which overwhelm the TDEs expected variability features, after considering the unique TDEs expected variability patterns. Based on theoretical TDEs expected variability plus AGN intrinsic variability randomly simulated by Continuous AutoRegressive process, long-term variability properties with and without TDEs contributions are well analyzed in AGN. Then, interesting effects of TDEs can be determined on long-term observed variability of AGN. First, more massive BHs, especially masses larger than $10^7 M_{\odot}$, can lead to more sensitive and positive dependence of τ_{TN} on R_{TN} , with τ_{TN} as variability timescale ratio of light curves with TDEs contributions to intrinsic light curves without TDEs contributions, and R_{TN} as ratio of peak intensity of TDEs expected variability to the mean intensity of intrinsic AGN variability without TDEs contributions. Second, stronger TDEs contributions R_{TN} can lead to τ_{TN} quite larger than 5. Third, for intrinsic AGN variability having longer variability timescales, TDEs contributions will lead τ_{TN} to be increased more slowly. The results actually provide an interesting forward-looking method to detect probable hidden TDEs in normal broad line AGN, due to quite different variability properties, especially different DRW/CAR process expected variability timescales, in different epochs, especially in normal broad line AGN with shorter intrinsic variability timescales and with BH masses larger than $10^7 M_{\odot}$.

Key words: active galaxies – active galactic nuclei - transient events - tidal disruption event

1 INTRODUCTION

Variability is one of fundamental characteristics of active galactic nuclei (AGN) (Rees 1984; Wagner & Witzel 1995; Ulrich, Maraschi & Urry 1997; Madejski & Sikora 2016; Dexter & Begelman 2019; Baldassare, Geha & Greene 2020; Burke et al. 2021). Although there is uncertain physical origin of the AGN variability with different timescales, such as the proposed different models in Torricelli-Ciamponi et al. (2000); Hawkins (2002); Favre, Courevoisier & Paltani (2005); Li & Cao (2008); Pechacek et al. (2013); Sartori et al. (2018); Panagiotou et al. (2022), etc, there is a preferred mathematical process to describe the long-term AGN variability, damped random walk (DRW) process or Continuous AutoRegressive (CAR) process with two basic process parameters of intrinsic variability timescale τ and amplitude σ . Kelly, Bechtold & Siemiginowska (2009) have firstly proposed the CAR process (Brockwell & Davis 2002) to described long-term AGN variability. And then, Kozłowski et al. (2010); Zu, Kochanek & Peterson (2011); Bailer-Jones (2012); Kelly et al. (2014); Simm et al. (2016); Takata, Mukuta & Mizumoto (2018); Moreno et al. (2019); Sheng, Ross & Nicholl (2022) have provided improved methods to estimate the process parameters.

There are many reported studies on the AGN variability through the DRW process. MacLeod et al. (2010) have modeled the variability of about 9000 spectroscopically confirmed quasars covered in the

SDSS Stripe82 region, and found correlations between the AGN parameters and the DRW process determined parameters. Bailer-Jones (2012) proposed an another fully probabilistic method for modeling AGN variability by the DRW process. Andrae, Kim & Bailer-Jones (2013) have shown that the DRW process is preferred to model AGN variability, rather than several other stochastic and deterministic models, by fitted results of long-term variability of 6304 quasars. Zu et al. (2013) have checked that the DRW process provided an adequate description of AGN optical variability across all timescales. Zhang & Feng (2017) have checked long-term variability properties of AGN with double-peaked broad emission lines, and found the difference in intrinsic variability timescales between normal broad line AGN and the AGN with double-peaked broad emission lines. Sanchez-Saez et al. (2018) have modeled variability by DRW process and reported statistical analysis of the connection between AGN variability and physical properties of the central AGN activities, through the 2345 sources detected in both SDSS (Sloan Digital Sky Survey) and QUEST-La Silla. Burke et al. (2020) have modeled the month-long, 30 minute-cadence, high-precision TESS (Transiting Exoplanet Survey Satellite) light curve by the DRW process in the well-known archetypical dwarf AGN NGC 4395. More recently, Suberlak, Ivezić & MacLeod (2021) have modeled 15years-long variability of 9248 quasars covered in SDSS stripe 82 region by combining the Pan-STARRS1 PS1 (Panoramic Survey Telescope and Rapid Response System 1 Survey) and SDSS light curves. Zhang et al. (2021a) have modeled long-term variability of a composite galaxy to provide clues to support a true Type-2 AGN. There-

^{*} Corresponding author Email: xgzhang@gxu.edu.cn

fore, the long-term AGN variability have been well accepted to be mathematically modeled by the DRW/CAR process.

Meanwhile, as discussed in [Mushotzky et al. \(2011\)](#); [Kasliwal et al. \(2015\)](#); [Guo et al. \(2017\)](#); [Tachibana et al. \(2020\)](#); [Stone et al. \(2022\)](#), intrinsic AGN variability deviations from the simple DRW description on short timescales, and also the estimated intrinsic variability timescale in the DRW process probably rises with increased baseline. However, in the manuscript, long-term variability not on short timescales but with the same length of time durations are mainly considered, therefore, neither variability on short timescales nor effects of different lengths of baseline are discussed in the manuscript. Besides the long-term intrinsic AGN variability well described by the CAR/DRW process, there is an unique kind of variability related to tidal disruption events (TDEs), which cannot intrinsically follow the CAR process expected variability properties, due to unique TDEs variability patterns. The well-known pioneer work on TDEs can be found in [Rees \(1988\)](#) and then followed in [Loeb & Ulmer \(1997\)](#); [Komossa et al. \(2004\)](#); [Lodato, King & Pringle \(2009\)](#); [Cenko et al. \(2012\)](#); [Guillochon & Ramirez-Ruiz \(2013\)](#); [Guillochon, Manukian & Ramirez-Ruiz \(2014\)](#); [Wang et al. \(2018\)](#); [Mockler, Guillochon & Ramirez-Ruiz \(2019\)](#); [Stone et al. \(2019\)](#); [Parkinson et al. \(2020\)](#); [Lynch & Ogilvie \(2021\)](#); [Zhou et al. \(2021\)](#); [Zhang \(2022\)](#), etc. The basic picture of a TDE is as follows. A star can be tidally disrupted by gravitational tidal force of a central massive black hole (BH), when it passing close to the central BH with a distance larger than event horizon of the BH but smaller than tidal disruption radius $R_T = R_\star \times (M_{\text{BH}}/M_\star)^{1/3}$ with R_\star , M_\star and M_{BH} as radius and mass of the being disrupted star and mass of central BH, respectively. The fallback materials can be accreted by the central massive BH, leading to time dependent TDEs variability roughly proportional to $t^{-5/3}$ at late times.

More recent reviews on theoretical simulations and/or observational results on TDEs can be found in [Komossa \(2015\)](#); [Lodato et al. \(2015\)](#); [Stone et al. \(2019\)](#). There are more than 100 TDE candidates reported in literature, see detail in <https://tde.space/>. Meanwhile, the well-known public sky survey projects have lead to more and more TDEs candidates detected, such as the TDEs candidates discovered through the known SDSS Stripe82 database in [van Velzen et al. \(2011\)](#), through the known Catalina Sky Survey (CSS, [Drake et al. \(2009\)](#)) in [Drake et al. \(2011\)](#), through the PanSTARRS (panoramic survey telescope and rapid response system) in [Gezari et al. \(2012\)](#); [Chornock et al. \(2014\)](#), through the PTF (palomar transient factory) in [Blagorodnova et al. \(2017\)](#); [van Velzen et al. \(2019\)](#), through the Optical Gravitational Lensing Experiment (OGLE) in [Wyrzykowski et al. \(2017\)](#); [Gromadzki et al. \(2019\)](#), through the ASAS-SN (all-sky automated survey for supernovae) in [Holoien et al. \(2014, 2016\)](#); [Hinkle et al. \(2021\)](#), through the CNSS (Caltech-NRAO Stripe 82 Survey) in [Anderson et al. \(2020\)](#), and through the ZTF (Zwicky Transient Facility) in [van Velzen et al. \(2019\)](#); [Lee et al. \(2020\)](#); [Stein et al. \(2021\)](#), etc. More recently, two large samples of dozens of new TDE candidates can be found in [van Velzen et al. \(2021\)](#) from the First Half of ZTF (Zwicky Transient Facility) Survey observations along with Swift UV and X-ray follow-up observations and in [Sazonov et al. \(2021\)](#) from the SRG all-sky survey observations and then confirmed by optical follow-up observations. More recent review on observational properties of reported TDEs can be found in [Gezari \(2021\)](#). However, among the reported TDEs candidates, there are few TDEs detected in normal broad line AGN with both apparent and strong intrinsic AGN variability.

Among the reported TDE candidates, especially optical TDE can-

didates, strong broad Balmer and Helium emission lines are fundamental spectroscopic characteristics, however, the detected broad emission lines are not expected to be tightly related to normal broad line regions in normal broad line AGN, but to be related to disk-like structures from TDE debris. The known cases with broad emission lines in TDEs candidates can be found in SDSS J0159 as discussed in [Merloni et al. \(2015\)](#); [Zhang \(2021b\)](#), ASASSN-14li as discussed in [Holoien et al. \(2016\)](#), PTF09djl as discussed in [Liu et al. \(2017\)](#), PS18kh as discussed in [Holoien et al. \(2019\)](#), AT2018hyz as discussed in [Short et al. \(2020\)](#); [Hung et al. \(2020\)](#), etc., indicating the reported broad emission lines in the TDE candidates are not related to normal BLRs in normal broad line AGN, but are tightly related to TDE debris. Moreover, there are several TDE candidates, their UV-band spectra have been well checked, such as the PS18kh, ASASSN-15lh, ASASSN-14li, etc., there are no broad Mg $\pi\lambda 2800\text{\AA}$ emission lines. And moreover, in the TDEs candidates with detected optical broad emission lines, there are no clues on DRW process expected variability, except the TDEs expected variability patterns. In other words, there are no confirmed evidence to support central TDEs in normal broad line AGN with apparent intrinsic AGN variability.

Certainly, not similar as in quiescent galaxies, a moving star can be tidally disrupted by the central supermassive BH without a pre-existing accretion disk. However, there is also an existed accretion disk around the central supermassive BH in AGN, therefore, effects of the existed accretion disk should be considered on accreting fallback TDEs debris in normal broad line AGN. [Kathirgamaraju et al. \(2017\)](#) have discussed effects of a pre-existing accretion disc on TDEs expected variability, leading to still TDE expected variability patterns but with a probable cut-off. [Chan et al. \(2019\)](#); [Chan, Piran & Krolik \(2020\)](#) have modeled TDEs variability in AGN with a pre-existing accretion disc, and discussed evolutions of the fallback bound debris being modified by collisions with the pre-existing disk, indicating the expected variability should be not totally similar as the TDEs expected variability patterns. However, there are so-far several TDEs candidates detected and reported in AGN. [Blanchard et al. \(2017\)](#) have reported a TDE candidate in a narrow line Seyfert 1 galaxy of which light curves can be roughly described by theoretical TDE model, and discussed that out-of-plane TDEs have quite weak interactions between the TDE debris and the pre-existing disk because the debris only intersect a small region of the disk. [Yan & Xie \(2018\)](#) have shown the TDE expected variability pattern in the low-luminosity AGN NGC 7213. [Liu et al. \(2020\)](#) have reported a TDE candidate in AGN SDSS J0227 with probable broad Balmer emission lines, and shown the sudden rise followed by a smooth decline trend in long-term variability in SDSS J0227. [Zhang et al. \(2022\)](#) have shown the TDE expected variability patterns in a narrow line Seyfert 1 galaxy. More recently, [Zhang \(2022b\)](#) have shown TDE expected long-term variability in the high redshift quasar SDSS J014124+010306, and [Zhang \(2022c\)](#) have discussed and shown TDE expected long-term variability of broad H α line luminosity in low luminosity broad line AGN NGC 1097. Therefore, totally similar TDE simulating variability can be expected in normal AGN with pre-existing accretion disks.

Rare TDEs reported in normal AGN are mainly due to stronger intrinsic AGN variability than TDEs variability. However, there are enough probabilities and feasibilities to expect TDEs in normal AGN with supermassive BHs, even there are no detected TDEs expected variability features which are probably overwhelmed by strong intrinsic AGN variability in observed light curves. For intrinsic long-term AGN variability, the expected timescales are simply consistent with accretion disk orbital timescales or thermal timescales of about hundreds of days as the shown results

in Kelly, Bechtold & Siemiginowska (2009) for normal AGN (including 55 AGN from the MACHO survey, 37 Palomar Green quasars, and eight Seyfert galaxies from the AGN Watch project), in Kozłowski et al. (2010) for about 2700 OGLE quasars, in MacLeod et al. (2010) for about 9000 quasars covered in the SDSS Stripe82 region, and in Rumbaugh et al. (2018) for extreme variability quasars. Meanwhile, for variability from probable TDEs around supermassive BHs with masses around $10^{7-8}M_{\odot}$ in AGN, the expected years-long timescales can be compared to the timescales of intrinsic long-term AGN variability. Therefore, it is interesting to check effects of TDEs on long-term AGN variability, which could provide interesting clues to expect probable hidden TDEs in normal broad line AGN with CAR process described intrinsic variability, through the long-term light curves from the public sky survey projects. Section 2 and Section 3 present our main hypotheses and main results. Section 4 gives the discussions and further applications. Section 5 gives our final conclusions. And in the manuscript, the cosmological parameters of $H_0 = 70 \text{ km} \cdot \text{s}^{-1} \text{ Mpc}^{-1}$, $\Omega_{\Lambda} = 0.7$ and $\Omega_{\text{m}} = 0.3$ have been adopted.

2 MAIN HYPOTHESES

2.1 Time Dependent Bolometric Luminosities from TDEs

In the manuscript, the well discussed theoretical TDEs model in Guillochon & Ramirez-Ruiz (2013); Guillochon, Manukian & Ramirez-Ruiz (2014); Mockler, Guillochon & Ramirez-Ruiz (2019) is mainly considered and accepted, combining with the mass-radius relation in Tout (1996) accepted for main-sequence stars. The time dependent bolometric luminosities from TDEs are simulated by the following four steps, similar as what we have done in Zhang (2022) to model X-ray variability of the relativistic TDE candidate Swift J2058.4+0516 and in Zhang (2022b,c) to model optical variability in quasar SDSS J014124+010306 and in low luminosity broad line AGN NGC 1097.

First, standard templates of viscous-delayed accretion rates in TDEs are created. Based on both the TDEFIT (<https://tde.space/tdefit/>) code (Guillochon, Manukian & Ramirez-Ruiz 2014) and the MOSFIT (Modular Open Source Fitter for Transients, <https://mosfit.readthedocs.io>) code (Guillochon et al. 2018) provided dm/de (m as debris mass and e the specific binding energy), templates of fallback material rate $\dot{M}_{fbt} = dm/de \times de/dt$ can be created for standard cases with the central BH mass $M_{\text{BH}} = 10^6 M_{\odot}$ and the being disrupted main-sequence star of $M_{\star} = 1 M_{\odot}$ and with a grid of the listed impact parameters β_t in Guillochon & Ramirez-Ruiz (2013). Considering the viscous delay as discussed in Guillochon & Ramirez-Ruiz (2013); Mockler, Guillochon & Ramirez-Ruiz (2019) by a parameter of viscous timescale T_{vis} , templates of viscous-delayed accretion rates \dot{M}_{at} can be determined by

$$\dot{M}_{at} = \frac{\exp(-t/T_{\text{vis}})}{T_{\text{vis}}} \int_0^t \exp(t'/T_{\text{vis}}) \dot{M}_{fbt} dt' \quad (1)$$

A grid of 31 evenly distributed $\log(T_{\text{vis}}, t/\text{years})$ range from -3 to 0 are applied to create templates \dot{M}_{at} for each impact parameter β_t . Therefore, the created templates \dot{M}_{at} include 736 (640) time-dependent viscous-delayed accretion rates for 31 different T_{vis} of each 23 (20) impact parameters β_t for the main-sequence star with polytropic index γ of 4/3 (5/3).

Second, for TDEs with model parameters of β and T_{vis} different

from the list values in β_t and in $T_{\text{vis}, t}$, the corresponding viscous-delayed accretion rates \dot{M}_a are created by the following two linear interpretations. Assuming that β_1, β_2 in the β_t are the two values nearer to the input β , and that $T_{\text{vis}1}, T_{\text{vis}2}$ in the $T_{\text{vis}, t}$ are the two values nearer to the input T_{vis} , the first linear interpretation is applied to find the viscous-delayed accretion rates with input T_{vis} but with $\beta = \beta_1$ and $\beta = \beta_2$ by

$$\begin{aligned} \dot{M}_a(T_{\text{vis}}, \beta_1) &= \dot{M}_{at}(T_{\text{vis}1}, \beta_1) + \\ &\frac{T_{\text{vis}} - T_{\text{vis}1}}{T_{\text{vis}2} - T_{\text{vis}1}} (\dot{M}_{at}(T_{\text{vis}2}, \beta_1) - \dot{M}_{at}(T_{\text{vis}1}, \beta_1)) \\ \dot{M}_a(T_{\text{vis}}, \beta_2) &= \dot{M}_{at}(T_{\text{vis}1}, \beta_2) + \\ &\frac{T_{\text{vis}} - T_{\text{vis}1}}{T_{\text{vis}2} - T_{\text{vis}1}} (\dot{M}_{at}(T_{\text{vis}2}, \beta_2) - \dot{M}_{at}(T_{\text{vis}1}, \beta_2)) \end{aligned} \quad (2)$$

The second linear interpretation is applied to find the viscous-delayed accretion rates with input T_{vis} and with input β by

$$\begin{aligned} \dot{M}_a(T_{\text{vis}}, \beta) &= \dot{M}_a(T_{\text{vis}}, \beta_1) + \\ &\frac{\beta - \beta_1}{\beta_2 - \beta_1} (\dot{M}_a(T_{\text{vis}}, \beta_2) - \dot{M}_a(T_{\text{vis}}, \beta_1)) \end{aligned} \quad (3)$$

Third, for TDEs with input parameters of M_{BH} and M_{\star} different from $10^6 M_{\odot}$ and $1 M_{\odot}$, the viscous-delayed accretion rates \dot{M} and the corresponding time information t in observer frame are created by the following scaling relations as shown in Guillochon, Manukian & Ramirez-Ruiz (2014); Mockler, Guillochon & Ramirez-Ruiz (2019),

$$\begin{aligned} \dot{M} &= M_{\text{BH}, 6}^{-0.5} \times M_{\star}^2 \times R_{\star}^{-1.5} \times \dot{M}_a(T_{\text{vis}}, \beta) \\ t &= (1+z) \times M_{\text{BH}}^{0.5} \times M_{\star}^{-1} \times R_{\star}^{1.5} \times t_a(T_{\text{vis}}, \beta) \end{aligned} \quad (4)$$

where $M_{\text{BH}, 6}$, M_{\star} , R_{\star} and z represent central BH mass in unit of $10^6 M_{\odot}$, stellar mass in unit of M_{\odot} , mass-radius relation determined stellar radius in unit of R_{\odot} , and redshift of host galaxy, respectively.

Fourth, the time dependent bolometric luminosities $L_{\text{bol}, t}$, TDE from TDEs \dot{M}_a can be finally calculated by

$$L_{\text{bol}, t, \text{TDE}} = \eta \times \dot{M}(t) c^2 \quad (5)$$

where c and η are the light speed and the energy transfer efficiency around central BH. The value η will be further discussed in the following subsections. Therefore, for a TDE with given model parameters of central BH mass M_{BH} , stellar mass M_{\star} and polytropic index γ of the central being disrupted main-sequence star, the impact parameter β , the viscous timescale T_{vis} , redshift z and energy transfer efficiency η , time dependent $L_{\text{bol}, t}$, TDE can be well simulated by the theoretical TDEs model.

Based on the four steps, TDE expected time dependent bolometric luminosities can be simulated by accepted the only criterion that the TDE model parameters determined tidal radius larger than the event horizon of central BH.

Before the end of the subsection, two points are noted. First, the circularizations in TDEs as discussed in Kochanek (1994); Bonnerot et al. (2016); Hayasaki, Stone & Loeb (2016); Zanazzi & Ogilvie (2020); Lynch & Ogilvie (2021) are not considered in the manuscript. The circularization emissions in TDEs have been probably detected in the TDE candidate ASASSN-15lh in Leloudas et al. (2016) and in TDE candidate AT 2019avd in Chen, Dou & Shen (2022), due to the two clear peaks (or two clear phases) detected in the NUV and/or optical band light curves. However, among the more than 100 reported TDEs candidates, there are rare TDEs candidates of which optical light curves have re-brightened peaks, indicating the ratio of TDEs with clear circularization emissions is very low. Therefore, we mainly consider the simple case

that the fallback timescales of the circularizations are significantly smaller than the viscous timescales of the accretion processes, and the fallback materials will circularize into a disk as soon as possible. Second, the expected plateau phase in TDEs expected light curves with considerations of pre-existing accretion disk of AGN are not considered in the manuscript, because the plateau phase has small time duration and/or no plateau phases in some AGN (such as the results in [Yan & Xie \(2018\)](#); [Zhang et al. \(2022\)](#); [Zhang \(2022b,c\)](#), etc.) due to low surface density of pre-existing accretion disk of AGN.

2.2 Time Dependent Bolometric Luminosities from the well-known AGN NGC5548

In the manuscript, the observed long-term light curve $L_{c, t, N5548}$ of continuum luminosity at 5100\AA over 13 years of the well-known broad line AGN NGC5548 ($z = 0.01717$) in [Peterson et al. \(2002\)](#) and in the AGNWATCH project (<https://www.asc.ohio-state.edu/astronomy/agnwatch/n5548/lcv/>) is collected as the AGN variability template. Then, the time dependent bolometric luminosity from NGC5548 $L_{bol, t, N5548} = 10 \times L_{c, t, N5548}$ is calculated by the bolometric corrections. The bolometric correction factor 10 is accepted, based on the statistical properties of spectral energy distributions of broad line AGN discussed in [Richards et al. \(2006\)](#); [Duras et al. \(2020\)](#) and also on the more recent discussed results in [Netzer \(2020\)](#).

Moreover, based on the well discussed results in [Peterson et al. \(2004\)](#); [Bentz et al. \(2010\)](#); [Pancoast et al. \(2014\)](#), the central BH mass can be accepted as $M_{BH} \sim 6.7 \times 10^7 M_{\odot}$ ¹ in the well-known reverberation mapped broad line AGN NGC5548 in the AGNWATCH project and in the LAMP (Lick AGN Monitoring Project) project (<https://www.physics.uci.edu/~barth/lamp.html>). And [Lu et al. \(2016\)](#) have reported similar BH mass of NGC5548 by the reverberation mapped results through Lijiang 2.4m telescope at Yunnan Observatory. More recently, [Williams et al. \(2020\)](#); [Horne et al. \(2021\)](#) have reported similar BH mass of NGC5548, through the space telescope and optical reverberation mapping project. Then, based on the well discussed results in [Davis & Laor \(2011\)](#), the energy transfer efficiency around the central BH in NGC5548 can be well estimated as

$$\eta = 0.089 \times \left(\frac{M_{BH}}{10^8 M_{\odot}} \right)^{0.52} = 7.2\% \quad (6)$$

which will be applied in Equation (5) above.

2.3 Time Dependent Bolometric Luminosities with considerations of both AGN and TDE

There are three kinds of mock light curves $L_{bol, t}$ created by AGN intrinsic variability plus TDEs contributions, from simplicity to complexity. The first kind is to simply add mock light curve $L_{bol, t, TDE}$ to the light curve $L_{bol, t, N5548}$. The second kind is to add mock light curve $L_{bol, t, TDE}$ to a randomly modified light curve $L_{bol, t, AGN}$ which is created by $L_{bol, t, N5548}$ plus a CAR process randomly created long-term variability. The third kind is created by CAR process randomly simulated long-term variability with different central physical properties.

The first kind of $L_{bol, t}$ are simply created as follows. Mock light curves $L_{bol, t, TDE}$ are created by randomly selected TDEs model

¹ BH mass values varying from $2 \times 10^7 M_{\odot}$ to $8 \times 10^7 M_{\odot}$ in NGC5548 have few effects on our final results.

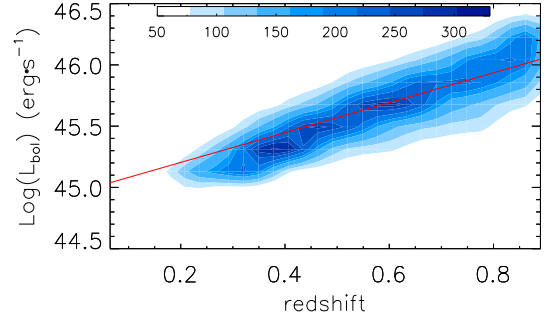


Figure 1. Dependence of bolometric luminosity (10 times of the continuum luminosity at 5100\AA) on redshift for all the collected SDSS quasars with reliable measurements of continuum luminosity from [Shen et al. \(2011\)](#). Solid red line shows the best description $L_{bol} = 44.96 + 1.22 \times z$.

parameters. The BH mass M_{BH} and η is fixed to $6.7 \times 10^7 M_{\odot}$ and 0.072 (the values of NGC5548). The stellar mass M_{\star} is randomly selected from $-2 < \log(M_{\star}/M_{\odot}) < 1$. The polytropic index γ is selected to be $4/3$ or $5/3$. The impact parameter is randomly selected from the minimum β_t to the maximum β_t . The viscous timescale T_{vis} is randomly selected from the minimum $T_{vis, t}$ to the maximum $T_{vis, t}$. Here, there is a criterion that the expected tidal radius

$$\frac{R_{TDE}}{R_s} = 5.06(M_{\star})^{-1/3} \left(\frac{M_{BH, 6}}{10} \right)^{-2/3} R_{\star} > 1 \quad (7)$$

larger than event horizon of central BH ($R_s = 2GM_{BH}/c^2$). Then, with $\gamma = 4/3$ ($\gamma = 5/3$), 1200 (1200) mock light curves $L_{bol, t, TDE}$ are randomly created. Considering TDEs with different starting times t_s randomly from 0 to 3000days, the mock $L_{bol, t}$ are created by

$$L_{bol, t} = L_{bol, t+t_s, TDE} + L_{bol, t, N5548} \quad (8)$$

Then, different white noises defined by signal-to-noise ratio (SNR) randomly from 30 to 80 are added to the mock light curves $L_{bol, t}$. And the observational uncertainties of $L_{bol, t, N5548}$ are accepted as the uncertainties of $L_{bol, t}$.

Before proceeding further, simple discussions are given to describe why values of SNRs for white noises are randomly selected from 30 to 80. As the collected information of the long-term light curve of NGC5548, the mean ratio of continuum emissions to uncertainties of continuum emissions is about 32. Meanwhile, to our knowledge, among our collected low-redshift ($z < 0.35$) SDSS (Sloan Digital Sky Survey) quasars, such as the sample discussed in [Zhang \(2023\)](#), the highest signal-to-noise ratio of SDSS spectra is about 74. Therefore, when adding white noises to the created mock light curves in the manuscript, corresponding SNRs are randomly selected from 30 to 80. Meanwhile, accepted SNRs from 30 to 80, corresponding photometric magnitude uncertainty can be simply estimated to be from 0.036mag to 0.013mag, which are similar as the magnitude uncertainties of light curves of quasars provided by SDSS Stripe82 database ([MacLeod et al. 2010](#)).

The second kind of $L_{bol, t}$ are created as follows. The mock light curves $L_{bol, t+t_s, TDE}$ are similarly created, but the AGN variability template $L_{bol, t, AGN}$ is created by

$$L_{bol, t, AGN} = L_{bol, t, N5548} + L(CAR) \quad (9)$$

where $L(CAR)$ is a randomly created light curve with mean of zero. And the $L(CAR)$ (with expected variance around 0.012) is randomly created through the CAR process described in

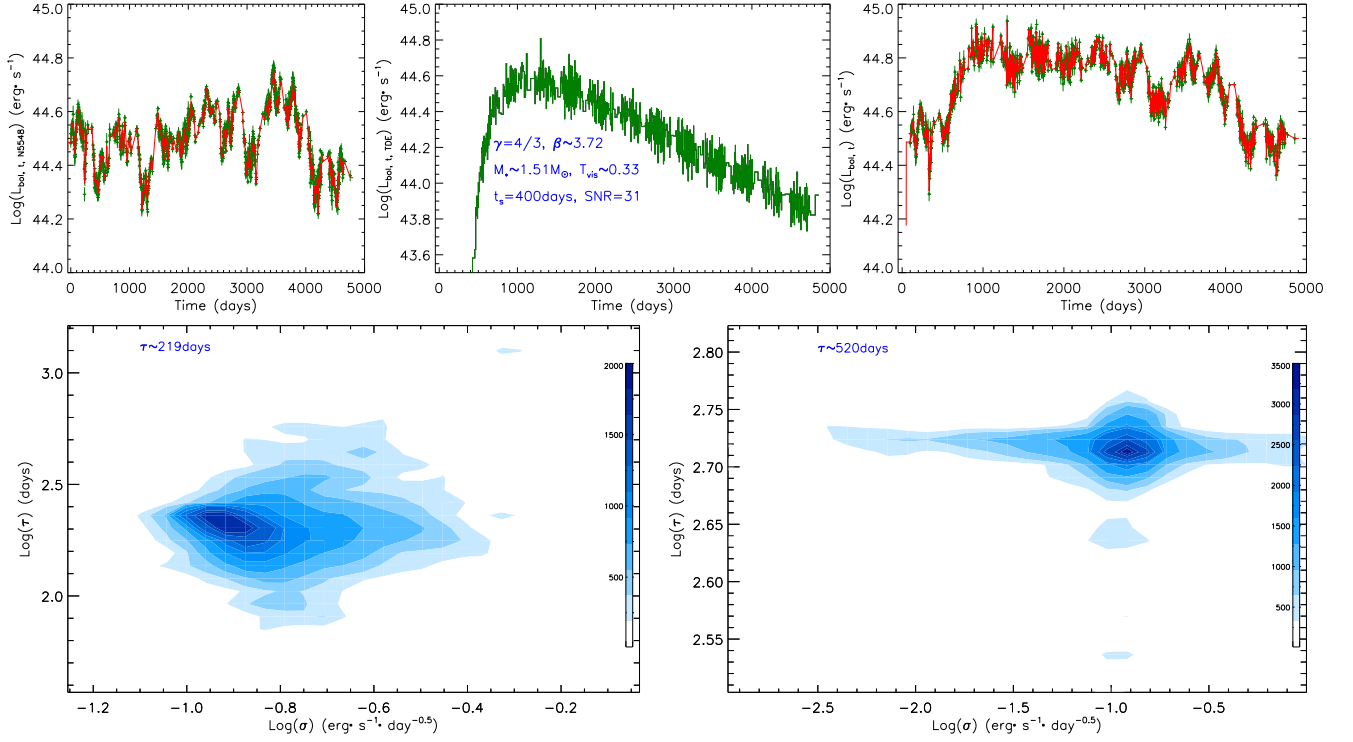


Figure 2. Top left panel shows $L_{\text{bol}, t, \text{N5548}}$ of NGC5548 (in dark green) and the kbs09 method determined best descriptions (solid red line). Bottom left panel shows the MCMC technique determined two-dimensional posterior distributions in contour of σ and τ of $L_{\text{bol}, t, \text{N5548}}$. Top middle panel shows an example of mock TDEs light curve $L_{\text{bol}, t, \text{TDE}}$ with model parameters marked in the panel. And due to small SNR, the light curve $L_{\text{bol}, t, \text{TDE}}$ is not smooth. Top right panel shows an example of mock light curve $L_{\text{bol}, t}$ (solid circles plus error bars in dark green) by $L_{\text{bol}, t, \text{N5548}}$ shown in the top left panel plus the $L_{\text{bol}, t, \text{TDE}}$ shown in the top middle panel, and the kbs09 method determined best descriptions (solid red line). Bottom right panel shows the MCMC technique determined two-dimensional posterior distributions in contour of σ and τ of $L_{\text{bol}, t}$ shown in the top-right panel.

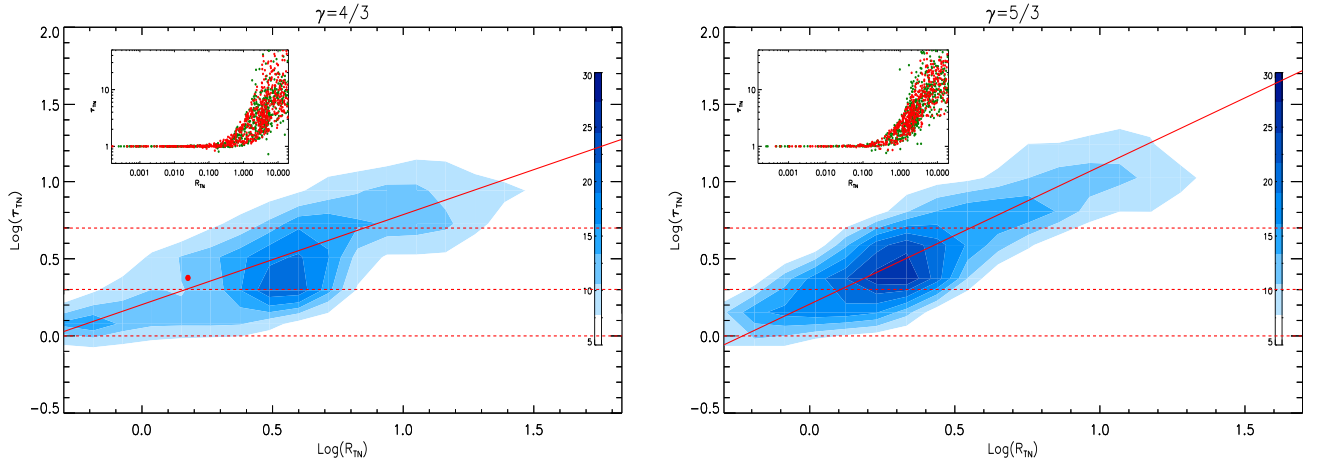


Figure 3. Dependence of τ_{TN} on R_{TN} and simple linear description in solid red line, based on the mock light curves $L_{\text{bol}, t}$ created by $L_{\text{bol}, t, \text{N5548}}$ plus contributions of TDEs with $\gamma = 4/3$ (in the left panel), and with $\gamma = 5/3$ (in the right panel). In left panel, solid red circle shows the results for the mock light curve $L_{\text{bol}, t}$ shown in the top right panel of Fig. 2. In each panel, top corner shows the results for all the 1200 mock light curves $L_{\text{bol}, t}$, however the contour is plotted for the cases with $R_{TN} > 0.5$. In each panel, from top to bottom, dashed red lines show $\tau_{TN} = 5, 2, 1$, respectively. And in each top corner, symbols in red and in dark green show the cases with SNR larger than 55 and smaller than 55, respectively. Meanwhile, in each top corner, due to dense data points, the error bars with uncertainties about 20% are not plotted.

Kelly, Bechtold & Siemiginowska (2009),

$$dL(CAR) = \frac{-1}{\tau}L(CAR)dt + \sigma\sqrt{dt}\epsilon(t) \quad (10)$$

where $\epsilon(t)$ a white noise process with zero mean and variance equal to 1. Here, the parameter τ is randomly selected from 100days to 1000days, as the shown results in MacLeod et al. (2010) for normal quasars. Then, the mock $L_{\text{bol}, t}$ are similarly created by

$$L_{\text{bol}, t} = L_{\text{bol}, t+\text{ts}, \text{TDE}} + L_{\text{bol}, t, \text{AGN}} \quad (11)$$

And different white noises defined by SNRs randomly from 30 to 80 are added to the mock light curves $L_{\text{bol}, t}$. Here, the light curve $L_{\text{bol}, t, \text{AGN}}$ has different intrinsic variability timescale and amplitude from those of $L_{\text{bol}, t, \text{N5548}}$, which will provide further considerations of effects of TDEs on long-term variability of AGN. And the observational uncertainties of $L_{\text{bol}, t, \text{N5548}}$ are accepted as the uncertainties of $L_{\text{bol}, t}$.

The third kind of $L_{\text{bol}, t}$ is mainly created as follows after considering different parameters of BH mass, redshift, energy transfer efficiency, etc. The AGN variability template $L_{\text{bol}, t, \text{CAR}}$ is created by the CAR process determined $L(CAR)$ plus an expected bolometric luminosity L_{b0} ($\log(L_{b0}/\text{erg/s})$) depending on redshift,

$$\begin{aligned} L_{\text{bol}, t, \text{CAR}} &= L_{b0} + L(CAR) \\ dL(CAR) &= \frac{-1}{\tau_0}L(CAR)dt + \sigma\sqrt{dt}\epsilon(t) \quad (12) \\ L_{b0} &= 44.96 + 1.22 \times z \end{aligned}$$

where τ_0 is selected to be 200days or 600days (a common value and a large value of intrinsic variability timescale in quasars, see results in MacLeod et al. (2010); Kelly, Bechtold & Siemiginowska (2009); Kozłowski et al. (2010); Rumbaugh et al. (2018)), and $\frac{\sigma^2\tau}{2}$ is selected to be around 0.012 (leading to similar variance as those in NGC5548). The selected parameters of τ and σ lead the $L(CAR)$ with mean of zero and variance similar as the $L_{\text{bol}, t, \text{N5548}}$. The dependence of bolometric luminosity on redshift $L_{b0} \propto 1.22 \times z$, shown in Fig. 1, is well determined from all the 23093 SDSS quasars in Shen et al. (2011) with measured continuum luminosity at 5100Å. There is a strong positive correlation between redshift and bolometric luminosity calculated by 10 times of the continuum luminosity at 5100Å, with Spearman rank correlation coefficient 0.66 ($P_{\text{null}} < 10^{-15}$) and with RMS scatter about 0.29. Here, 6 different values of 0.05, 0.1, 0.2, 0.3, 0.5, 1 are accepted as input redshift, applied to determine L_0 . Meanwhile, based on the three different BH masses $M_{\text{BH}} = 10^6, 10^7, 5 \times 10^7 M_{\odot}$, three different energy transfer efficiency $\eta = 0.06, 0.15, 0.3$ and the six redshift, the $L_{\text{bol}, t+\text{ts}, \text{TDE}}(M_{\text{BH}}, \eta, z)$ can be randomly created. Then, the mock light curves $L_{\text{bol}, t}$ are similarly created by

$$L_{\text{bol}, t} = L_{\text{bol}, t+\text{ts}, \text{TDE}}(M_{\text{BH}}, \eta, z) + L_{\text{bol}, t, \text{CAR}} \quad (13)$$

And different white noises defined by SNRs randomly from 30 to 80 are added to the mock light curves $L_{\text{bol}, t}$. For each series $[\gamma, M_{\text{BH}}, \eta, z, \tau]$, 1200 mock light curves are created with contributions of TDEs. Finally, there are $2 \times 3 \times 3 \times 6 \times 2 \times 1200 = 259200$ mock light curves created after considering TDEs contributions to intrinsic AGN variability. And 10% are accepted as the uncertainties of $L_{\text{bol}, t}$.

Actually, besides the linear dependence of bolometric luminosity on redshift, dependence of BH mass on redshift is also checked through the reported parameters of the quasars in Shen et al. (2011). However, the Spearman Rank correlation coefficient for the dependence is only 0.29, quite weaker than the dependence of bolometric luminosity on redshift. Therefore, rather than dependence

of BH mass on redshift, the linear dependence of bolometric luminosity on redshift is accepted in the manuscript. The application of the linear dependence of bolometric luminosity on redshift can reduce one free model parameter to create the third kind of mock light curves. Moreover, as shown in MacLeod et al. (2010); Kelly, Bechtold & Siemiginowska (2009), there is a dependence of process parameter τ on BH mass. However, the dependence is very loose, with Spearman Rank correlation coefficient about 0.23. Therefore, in the manuscript, the loose dependence of process parameter τ on BH mass is not accepted. And accepted the BH mass and τ and redshift are independent parameters, much wider parameter space can be occupied to create the mock light curves, and more efficient conclusions can be obtained.

Before the end of the section, three points are noted. First and foremost, in order to clearly show properties of model parameters applied to create TDEs contributions and to create $L(CAR)$, Table 1 shows the accepted values and/or accepted ranges of the applied model parameters. Besides, the main objective of the manuscript is to determine effects of TDEs contributions on observed long-term AGN variability from simplicity to complexity. Therefore, when the first kind and the second kind of mock light curves are created, the oversimplified procedure is firstly applied with the fixed BH mass (the BH mass of NGC5548), the fixed energy transfer efficiency (determined by the BH mass of NGC5548) and the fixed redshift (the redshift of NGC5548). Then, effects of randomly selected values of model parameters are considered through the third kind of mock light curves. Last but not the least, for the three kinds of mock light curves $L_{\text{bol}, t}$, the corresponding maximum BH mass is $6.7 \times 10^7 M_{\odot}$ (the BH mass of NGC5548), which is a large (near to the Hills mass limit) but reasonable value, see the maximum BH mass about $66 \times 10^6 M_{\odot}$ determined by the MOSFIT in TDEs candidates in Mockler, Guillochon & Ramirez-Ruiz (2019). Meanwhile, when the third kind of mock light curves are created, the Equation (6) is not applied to determined energy transfer efficiency, after considering the listed values of η in Mockler, Guillochon & Ramirez-Ruiz (2019) that high η could be expected around central BH with masses around $10^6 M_{\odot}$. And also as the shown results in Mockler, Guillochon & Ramirez-Ruiz (2019), the collected η values from 0.06 to 0.3 are also reasonable to create time dependent TDEs expected bolometric luminosities for the third kind of mock light curves.

3 MAIN RESULTS

3.1 Results based on the Long-Term Variabilities of

$$L_{\text{bol}, t, \text{N5548}}$$

As the discussed results in Kelly, Bechtold & Siemiginowska (2009) (see their Fig. 4), the long-term variability $L_{\text{bol}, t, \text{N5548}}$ of NGC5548 has intrinsic variability timescale about 214days. The same method as shown in Equation (7)-(12) in Kelly, Bechtold & Siemiginowska (2009) (the kbs09 method) is applied to analyze variability of $L_{\text{bol}, t, \text{N5548}}$, in order to ensure the applied kbs09 method in the manuscript is reliable. Here, rather than the public JAVELIN (Just Another Vehicle for Estimating Lags In Nuclei) code in Zu, Kochanek & Peterson (2011); Zu et al. (2013), the kbs09 method is applied in the manuscript, due to the following main reason. For each mock light curve with about 1500 data points (time duration longer than 10 years), the kbs09 method running in Surface Studio2 can give the final best-fitting results in ten minutes through the Levenberg-Marquardt least-squares minimization technique (the

Table 1. Model Parameters applied to create the three kinds of mock light curves

	parameters applied in TDE model with $\gamma = 4/3, 5/3$							parameters for $L(CAR)$	
	M_{BH}	$\log(M_\star)$	η	z	β	$\log(T_{vis})$	t_s	τ	$\frac{\sigma^2\tau}{2}$
1st	6.7×10^7	$\in[-2, 1]$	0.072	0.01717	$\in[\beta_l, \beta_m]$	$\in[-3, 0]$	$\in[0, 3000]$
2nd	6.7×10^7	$\in[-2, 1]$	0.072	0.01717	$\in[\beta_l, \beta_m]$	$\in[-3, 0]$	$\in[0, 3000]$	$\in[100, 1000]$	$\in[0.003, 0.048]$
3rd	$\subset[10^6, 10^7, 5 \times 10^7]$	$\in[-2, 1]$	$\subset[0.06, 0.15, 0.30]$	$\subset[0.05, 0.1, 0.2, 0.3, 0.5, 1.0]$	$\in[\beta_l, \beta_m]$	$\in[-3, 0]$	$\in[0, 3000]$	$\subset[200, 600]$	$\in[0.003, 0.048]$

- 1: The first column shows which kind of mock light curves, '1st' means the first kind of mock light curve $L_{bol, t} = L_{bol, t+ts, TDE} + L_{bol, t, N5548}$, '2nd' means the second kind of mock light curve $L_{bol, t} = L_{bol, t+ts, TDE} + L_{bol, t, N5548} + L(CAR)$ (with $L(CAR)$ as CAR process created variability), '3rd' means the third kind of mock light curve $L_{bol, t} = L_{bol, t+ts, TDE}(M_{BH}, \eta, z) + L_{bol, t, CAR}$.
- 2: The second column, the third column, the fourth column, the fifth column, the sixth column, the seventh column and the eighth column show the parameters of BH mass in units of M_\odot , logarithmic stellar mass in units of M_\odot , energy transfer efficiency η , redshift z , β , logarithmic T_{vis} in units of years and shifted time in units of days, applied in theoretical TDE model.
- 3: The last two panels show the CAR process parameters of τ in units of days and $\frac{\sigma^2\tau}{2}$ (expected variance of the CAR created light curve) applied to created light curves $L(CAR)$.
- 4: In each cell for the parameters, if there is only one value, meaning that the parameter is fixed to the listed value.
- 5: In each cell for the parameters, if the mathematical symbol \in is used, meaning that the parameter is randomly selected from the minimum value to the maximum value listed in the square brackets following the mathematical symbol \in .
- 6: In each cell for the parameters, if the mathematical symbol \subset is used, meaning that value of the parameter is chosen from the values listed in the square brackets following the mathematical symbol \subset .
- 7: In the last column, the parameter $\frac{\sigma^2\tau}{2}$ shows the expected variance of the CAR process created light curve. Based on the variance 0.012 of the light curve of NGC5548, the $\frac{\sigma^2\tau}{2}$ is accepted to be larger than 0.25×0.012 and smaller than 4×0.012 for the created $L(CAR)$ in the second kind and the third kind of mock light curves.
- 8: In the fifth column, the β is randomly selected from 0.6 to 4 if $\gamma = 4/3$, and randomly selected from 0.5 to 2.5 if $\gamma = 5/3$.

known MPFIT package, Markwardt 2009), however, the JAVELIN code will give the final results in more than one hour.

The $L_{bol, t, N5548}$ is shown in top left panel of Fig. 2, with the kbs09 method determined best descriptions through the Maximum Likelihood method combining with the Markov Chain Monte Carlo (MCMC) technique (Foreman-Mackey et al. 2013), with the kbs09 method determined process parameters through the MPFIT package accepted as starting values of the process parameters in the MCMC technique. The determined posterior distributions of the parameters of τ and σ are shown in the bottom left panel of Fig. 2, with accepted $\log(\tau/days) \sim 2.34^{+0.107}_{-0.076}$ ($\tau \sim 219^{+60}_{-36}$ days) which is well consistent with the reported 214days in Kelly, Bechtold & Siemiginowska (2009). Therefore, the applied kbs09 method is reliable enough.

Through the kbs09 method applied through the Levenberg-Marquardt least-squares minimization technique, variability properties, especially the CAR process parameters of σ and τ , can be well determined for the total 2400 mock light curves $L_{bol, t}$ created by $L_{bol, t, N5548}$ plus $L_{bol, t, TDE}$. Top middle panel and top right panel of Fig. 2 show an example of $L_{bol, t, TDE}$ and an example of $L_{bol, t}$. For the shown example in top right panel of Fig. 2 without clear TDEs expected variability features, the determined variability timescale is about 520days, as the shown posterior distributions in bottom right panel of Fig. 2 determined by MCMC technique applied in the kbs09 method, significantly longer than the intrinsic 219days of NGC5548, indicating TDEs contributions can lead to larger variability timescales.

In order to show clearer effects of TDEs contributions, two parameters R_{TN} and τ_{TN} are defined, R_{TN} as ratio of the peak intensity of $L_{bol, t, TDE}$ to the mean intensity of $L_{bol, t, N5548}$, and τ_{TN} as ratio of the variability timescale of $L_{bol, t}$ to the intrinsic variability timescale 219days of $L_{bol, t, N5548}$. Then, Fig. 3 shows the dependence of τ_{TN} on R_{TN} of the 2400 mock light curves $L_{bol, t}$, 1200 light curves based on the $L_{bol, t, TDE}$ created with $\gamma = 4/3$ and 1200 light curves based on the $L_{bol, t, TDE}$ created with $\gamma = 5/3$. For $R_{TN} > 0.5$ (stronger TDEs contributions), there are positive

correlations between τ_{TN} on R_{TN} , with the Spearman rank correlation coefficient is about 0.71 (0.79) with $P_{null} < 10^{-15}$ for the cases with $\gamma = 4/3$ ($\gamma = 5/3$). Here, the critical value $R_{TN} > 0.5$ is simply determined that the variance of τ_{TN} of the data points with $R_{TN} > 0.5$ is at least 2000 times larger than the variance of τ_{TN} of the data points with $R_{TN} < 0.5$. Actually, small different critical values from 0.5 have few effects on the discussed results. After considering the uncertainties in both coordinates, the positive dependence with $R_{TN} > 0.5$ can be simply described by

$$\begin{aligned} \log(\tau_{TN})(\gamma = 4/3) &= 0.20 + 0.58 \log(R_{TN}) \\ \log(\tau_{TN})(\gamma = 5/3) &= 0.21 + 0.89 \log(R_{TN}) \end{aligned} \quad (14)$$

through the FITEXY code (<https://idlastro.gsfc.nasa.gov/ftp/pro/mat>) written by Frank Varosi) as discussed in Tremaine et al. (2002). It is clear that longer variability timescales can be confirmed with larger TDEs contributions. And SNRs have few effects on the results, based on the shown results in each top corner in each panel of Fig. 3.

Before end of the subsection, scatters of τ_{TN} for given R_{TN} can be simply discusses as follows. For smaller values of R_{TN} , TDEs contributions are very tiny, leading to few effects of TDEs contributions on determined τ in mock light curves, indicating tiny scatters of τ_{TN} . However, for larger values of R_{TN} leading to apparent TDEs contributions, different values of stellar mass and β and large value T_{vis} can lead to quite different time durations of TDE expected light curves with the same peak intensity. The different time durations can lead to different ratios of τ_{TN} . Unless the model parameters applied in TDE model are fixed for a given R_{TN} , the scatters of R_{TN} can be well expected, and provide robust clues in the manuscript to detect hidden TDEs in broad line AGN with apparent intrinsic variability. Similar scatters of τ_{TN} can also be expected in the following subsections.

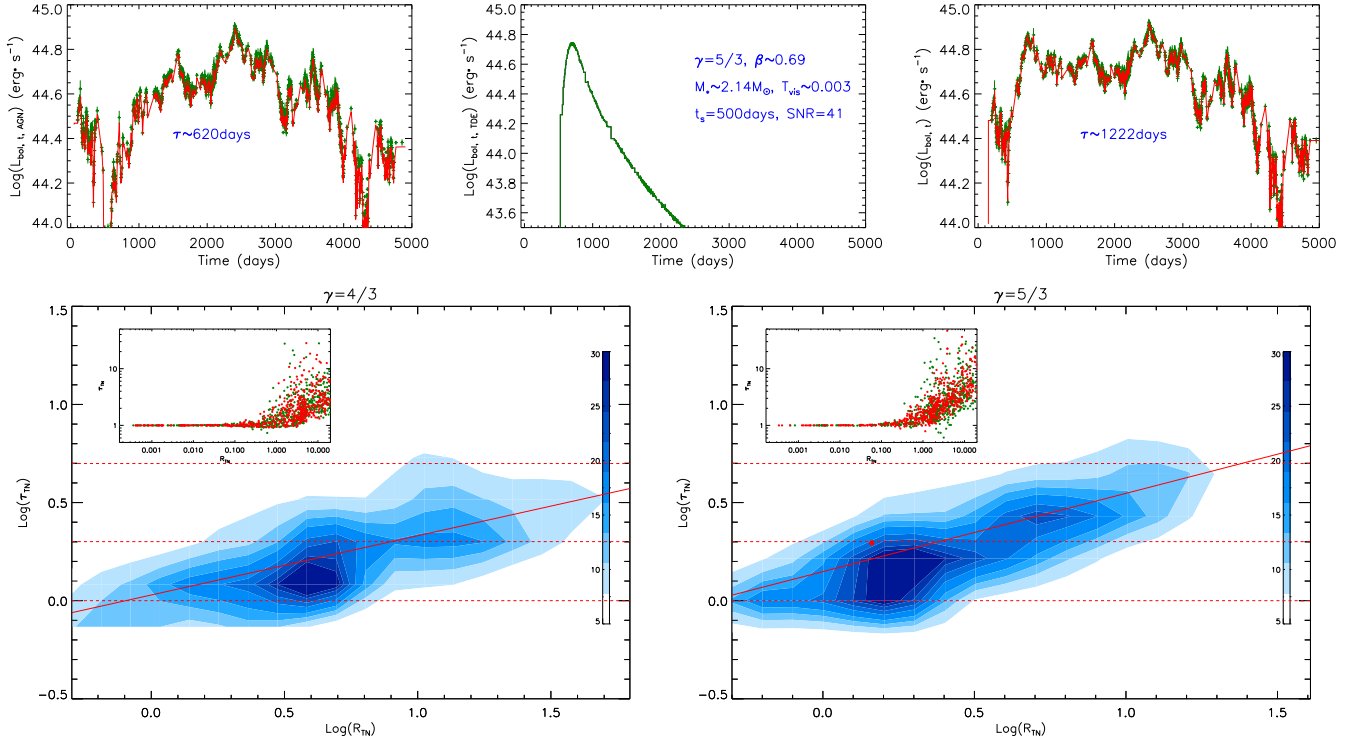


Figure 4. Top panels show the results similar as those shown in top panels of Fig. 2, but based on the light curve $L_{bol, t, AGN}$ shown in the top left panel. Bottom panels show the results similar as those in Fig. 3, but based on the light curve $L_{bol, t, AGN}$ with intrinsic variability timescale about 620days. In the bottom right panel, the solid red circle shows the results for the mock light curve $L_{bol, t}$ shown in the top right panel. In top corners of bottom panels, due to large number of dense data points, the error bars with uncertainties about 20% are not plotted.

3.2 Results based on the Long-Term Variabilities of $L_{bol, t, AGN}$

Similar as the results on $L_{bol, t, N5548}$, top panels of Fig. 4 show an example of mock light curve $L_{bol, t, TDE}$ (in middle panel) and an example of mock light curve $L_{bol, t}$ (in right panel) created by $L_{bol, t, AGN}$ shown in the left panel plus the $L_{bol, t, TDE}$ shown in the middle panel. And the kbs09 method is applied to determine the intrinsic variability timescale of $L_{bol, t, AGN}$ as $\tau \sim 620$ days through the Levenberg-Marquardt least-squares minimization technique. Bottom panels of Fig. 4 shows the dependence of τ_{TN} on R_{TN} of the 2400 mock light curves $L_{bol, t}$ based on the $L_{bol, t, AGN}$. For $R_{TN} > 0.5$, the Spearman rank correlation coefficient is about 0.63 (0.68) with $P_{null} < 10^{-15}$ for the cases with $\gamma = 4/3$ ($\gamma = 5/3$). The positive dependence with $R_{TN} > 0.5$ can be simply described by

$$\begin{aligned} \log(\tau_{TN})(\gamma = 4/3) &= 0.03 + 0.30 \log(R_{TN}) \\ \log(\tau_{TN})(\gamma = 5/3) &= 0.15 + 0.40 \log(R_{TN}) \end{aligned} \quad (15)$$

through the same FITEXY code.

Similar results can be found that longer variability timescales can be confirmed with larger TDEs contributions, and SNRs have few effects on the results. However, the intrinsic AGN variability have longer variability timescales, the τ_{TN} will increase more slowly, based on the smaller slopes shown in the equations above.

3.3 Results based on the Long-Term Variabilities of $L_{bol, t, CAR}$

In the subsection, it is interesting to check effects of different model parameters on the dependence of τ_{TN} on R_{TN} which are determined through the MPFIT package applied in the kbs09 method.

Fig. 5 show two examples of the mock light curves $L_{bol, t}$ with different input model parameters marked in each panel. The first shown $L_{bol, t}$ is created with $\tau_0 = 200$ days, $M_{BH} = 10^6 M_{\odot}$, $z = 0.05$, $\gamma = 4/3$, $\beta \sim 1.55$, $M_* \sim 0.31 M_{\odot}$, $T_{vis} \sim 0.218$, $t_s \sim 2200$ days, SNR = 46, $\eta = 0.06$. The second shown $L_{bol, t}$ is created with $\tau_0 = 600$ days, $M_{BH} = 5 \times 10^7 M_{\odot}$, $z = 1.0$, $\gamma = 5/3$, $\beta \sim 1.32$, $M_* \sim 8.32 M_{\odot}$, $T_{vis} \sim 0.085$, $t_s \sim 1500$ days, SNR = 30, $\eta = 0.3$. Before proceeding further, there is a more intuitive result that smaller variability timescale of TDEs variability from cases with smaller BH mass should have few effects on R_{TN} , such as the shown results with tiny changes in timescales in top panels of Fig. 5. More detailed results are shown as follows.

Fig. 6 shows the dependence of τ_{TN} on R_{TN} for the cases (cases-6-2-4, the first number '6' means BH mass as $10^6 M_{\odot}$, the second number '2' means $\tau_0/100$ days = 2, and the third number '4' means $\gamma \times 3 = 4$) with $M_{BH} = 10^6 M_{\odot}$, $\tau_0 = 200$ days, and $\gamma = 4/3$. It is clear that TDEs contributions around BHs with masses around $10^6 M_{\odot}$ have few effects on the dependence of τ_{TN} on R_{TN} , all results shown in Fig. 6 with Spearman rank correlation coefficients smaller than 0.3 for the data points with $R_{TN} > 1$, even considering different redshift and different η . The results can be well expected due to smaller variability timescales of TDEs around BHs with masses around $10^6 M_{\odot}$, relative to the long time durations of $L_{bol, t, CAR}$. Besides the results for the cases-6-2-4, there are totally

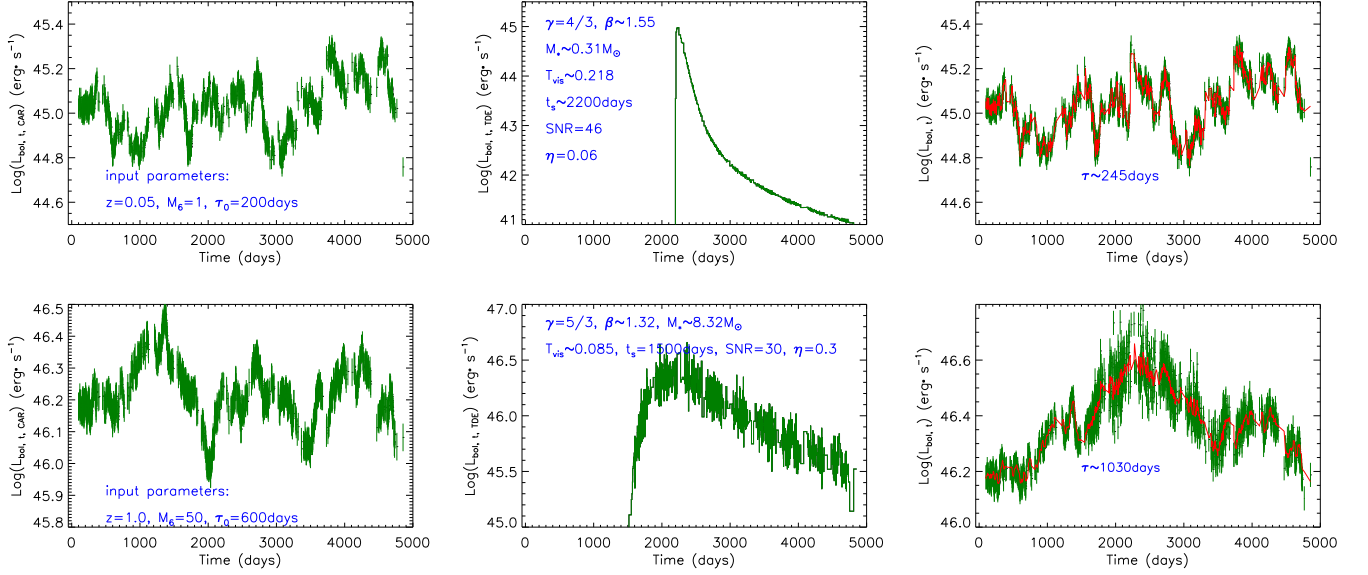


Figure 5. Two examples on the mock light curves $L_{\text{bol},t,\text{CAR}}$ shown as dots plus error bars in dark green in left panels, the mock light curves $L_{\text{bol},t,\text{TDE}}(M_{\text{BH}}, \eta, z)$ shown in the middle panels and the mock light curves $L_{\text{bol},t}$ shown as dots plus error bars in dark green in the right panels. In each left panel, the input model parameters of BH mass M_6 (in unit of $10^6 M_\odot$), redshift, τ_0 are listed in blue characters. In each middle panel, the input TDEs model parameters of γ, β , stellar mass M_* , T_{vis} , t_s , SNR and η are listed in blue characters. In each right panel, solid red line shows the kbs09 method determined best descriptions to the $L_{\text{bol},t}$, and the corresponding determined timescale τ is listed in blue characters.

similar results, no apparent positive dependence of τ_{TN} on R_{TN} , for the cases (cases-6-6-4) with $M_{\text{BH}} = 10^6 M_\odot$, $\tau_0 = 600$ days, and $\gamma = 4/3$, and for the cases (cases-6-2-5) with $M_{\text{BH}} = 10^6 M_\odot$, $\tau_0 = 200$ days, and $\gamma = 5/3$, and for the cases (cases-6-6-5) with $M_{\text{BH}} = 10^6 M_\odot$, $\tau_0 = 600$ days, and $\gamma = 5/3$. Therefore, we do not show the results on cases-6-6-4, cases-6-2-5, and cases-6-6-5 in plots. And there are no further discussions on the results with $M_{\text{BH}} = 10^6 M_\odot$, but the determined Spearman rank correlation coefficients are listed in Table 2 for all the cases with BH mass $10^6 M_\odot$. In one word, contributions of TDEs around BHs with masses $10^6 M_\odot$ cannot provide clear clues on central TDEs, through long-term variability.

Then, similar as the discussed results on dependence of τ_{TN} on R_{TN} for the cases with $M_{\text{BH}} = 10^6 M_\odot$, the results on the dependence of τ_{TN} on R_{TN} are also discussed with BH masses as $10^7 M_\odot$ and $5 \times 10^7 M_\odot$. Based on two different values of M_{BH} , two different values of τ_0 and two different values of γ , there are 8 cases named as cases-7-2-4 (the first number '7' means BH mass as $\log(M_{\text{BH}}/M_\odot) = 7$, the second number '2' means $\tau_0/100$ days = 2, and the third number '4' means $\gamma \times 3 = 4$), cases-7-6-4, cases-7-2-5, cases-7-6-5, cases-7-7-2-4 (the first number '7.7' means BH mass as $\log(M_{\text{BH}}/M_\odot) = \log(5 \times 10^7) \sim 7.7$), cases-7-7-6-4, cases-7-7-2-5, cases-7-7-6-5. Then, similar as the discussed results for the 18×4 dependences for the four cases with $M_{\text{BH}} = 10^6 M_\odot$, all the $144 (18 \times 8)$ dependences of τ_{TN} on R_{TN} for $R_{\text{TN}} > R_{\text{cri}}$ are carefully checked in all the cases with $M_{\text{BH}} = 10^7 M_\odot, 5 \times 10^7 M_\odot$. Here, the critical values $R_{\text{cri}} = 0.3$ and $R_{\text{cri}} = 0.15$ are simply determined and accepted for the cases with $M_{\text{BH}} = 10^7 M_\odot$ and with $M_{\text{BH}} = 5 \times 10^7 M_\odot$, respectively, after simply considering the variance of τ_{TN} of the data points with $R_{\text{TN}} > R_{\text{cri}}$ at least 2000 times larger than the variance of τ_{TN} of the data points with $R_{\text{TN}} < R_{\text{cri}}$. The determined Spearman Rank Correlation coefficients are listed in Table 2. Meanwhile, for the correlations with correlation coefficients

larger than 0.3, through the same FITEXY code, the strong positive correlations between τ_{TN} and R_{TN} for $R_{\text{TN}} > 0.3$ can be well described by

$$\log(\tau_{\text{TN}}) = A + B \times \log(R_{\text{TN}}) \quad (16)$$

with determined B also listed in Table 2.

Here, not all the $144 (18 \times 8)$ dependences of τ_{TN} on R_{TN} are shown in plots, but the dependence with maximum Spearman Rank correlation coefficient is shown in Fig. 7 among the 18 dependences in each case with $M_{\text{BH}} = 10^7 M_\odot, M_{\text{BH}} = 5 \times 10^7 M_\odot$. Meanwhile, based on the determined Coefficients and the slope B (if there was) listed in Table 2 for the 216 dependences in the 12 cases with $M_{\text{BH}} = 10^6 M_\odot, M_{\text{BH}} = 10^7 M_\odot, M_{\text{BH}} = 5 \times 10^7 M_\odot$, properties of Coefficients and slope B are shown in Fig. 8.

Based on the determined Coefficients listed in Table 2 and the shown results in Fig. 8, the following seven points can be found. First, comparing with the cases with $M_{\text{BH}} = 10^6 M_\odot$, there are more sensitive and clearer positive dependence of τ_{TN} on R_{TN} ($R_{\text{TN}} > 0.3$), due to the results with Spearman rank correlation coefficients larger than 0.3: almost all the cases with input $\tau_0 = 200$ days and $M_{\text{BH}} = 10^7 M_\odot$ have coefficients larger than 0.3 for the correlations with $R_{\text{TN}} > 0.3$. Second, for the cases with $M_{\text{BH}} = 10^7 M_\odot$, intrinsic variability timescales long as 600days should lead to no clear positive dependence of τ_{TN} on R_{TN} , but intrinsic variability timescales long as 200days can lead to clear positive dependence of τ_{TN} on R_{TN} . Third, for the cases with $M_{\text{BH}} = 10^7 M_\odot$, the positive dependence of τ_{TN} on R_{TN} are steeper (larger B) in the cases with $\gamma = 5/3$ than with $\gamma = 4/3$. Fourth, comparing with cases with $M_{\text{BH}} = 10^6 M_\odot$ and $M_{\text{BH}} = 10^7 M_\odot$, there are more sensitive and clearer positive dependence of τ_{TN} on R_{TN} for the cases with $M_{\text{BH}} = 5 \times 10^7 M_\odot$, due to the results with Spearman rank correlation coefficients larger than 0.3: all the cases with input $\tau_0 = 200$ days and half of the cases with $\tau_0 = 600$ days have

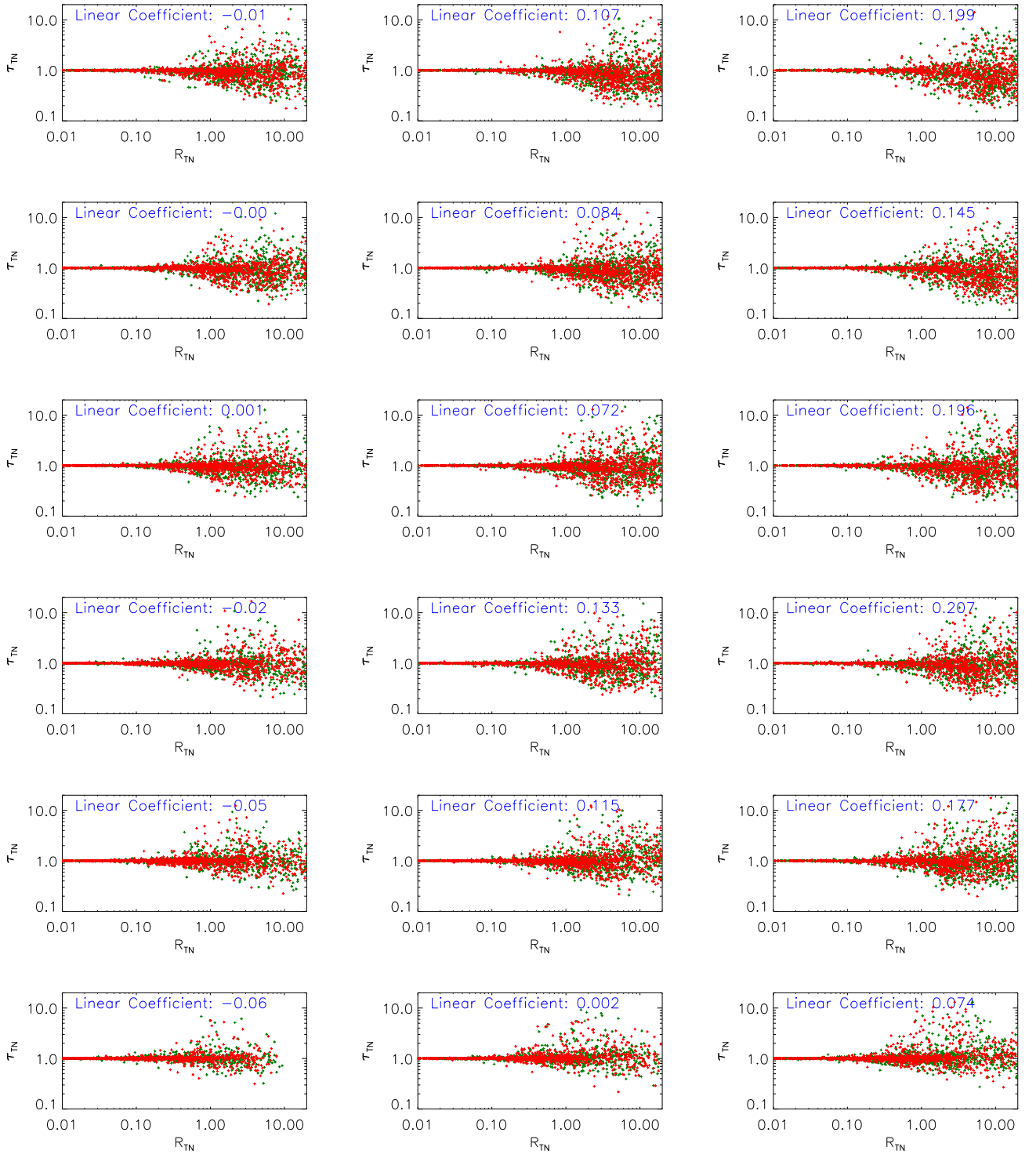


Figure 6. On the dependence of τ_{TN} on R_{TN} for the mock light curves based on the long-term variability $L_{bol, t, CAR}$ created with $M_{BH} = 10^6 M_{\odot}$, $\tau_0 = 200$ days plus the $L_{bol, t, TDE}$ created with $\gamma = 4/3$. For the panels from top to bottom, the results are based on the redshift of 0.05, 0.1, 0.2, 0.3, 0.5, and 1.0, respectively. For the panels from left to right, the results are based on the η of 0.06, 0.15 and 0.3, respectively. In each panel, the Spearman rank correlation coefficient for the correlation between τ_{TN} and R_{TN} ($R_{TN} > 1$) is listed in blue characters. In each panel, pluses in red and in dark green show the results with SNR larger than 55 and smaller than 55, respectively. In each panel, due to large number of dense data points, the error bars with uncertainties about 20% - 25% are not plotted.

coefficients larger than 0.3 for the correlation with $R_{TN} > 0.15$. Fifth, for the cases with BH masses about $5 \times 10^7 M_{\odot}$, intrinsic variability timescales long as 600days but only with $\gamma = 5/3$ should lead to clear positive dependence of τ_{TN} on R_{TN} , but intrinsic variability timescales long as 200days almost can lead to clear positive dependence of τ_{TN} on R_{TN} . Sixth, the positive dependence of τ_{TN} on R_{TN} are steeper (larger B) in the cases with $\gamma = 5/3$ than with $\gamma = 4/3$. Seventh, there are few effects of SNR on dependences of τ_{TN} on R_{TN} , such as the shown results in Fig. 7.

Based on the results above, we can find that

- BH mass has apparent effects on the dependence of τ_{TN} on R_{TN} . Larger BH masses can lead to more apparent and steeper dependence of τ_{TN} on R_{TN} .
- Polytropic index γ has apparent effects on the dependence of τ_{TN} on R_{TN} . $\gamma = 5/3$ can lead to more apparent and steeper dependence of τ_{TN} on R_{TN} .
- Redshift has tiny effects on the dependence of τ_{TN} on R_{TN} . At least, redshift changing from 0.05 to 1.0 cannot lead to clear changes in the dependence of τ_{TN} on R_{TN} , only parameter B being increased quite smoothly in cases-7.2-5 (with $M_{BH} = 10^7 M_{\odot}$, $\tau_0 = 200days$ and $3 \times \gamma = 5$), cases-7.7-2-4 (with $M_{BH} = 5 \times 10^7 M_{\odot}$, $\tau_0 = 200days$ and $3 \times \gamma = 4$), cases-7.7-2-5 (with $M_{BH} = 5 \times 10^7 M_{\odot}$, $\tau_0 = 200days$ and $3 \times \gamma = 5$) and cases-7.7-6-5 ($M_{BH} = 5 \times 10^7 M_{\odot}$, $\tau_0 = 600days$ and $3 \times \gamma = 5$).
- Energy transfer efficiency has tiny effects on the dependence of τ_{TN} on R_{TN} . At least, energy transfer efficiency changing from 0.06 to 0.3 cannot lead to clear changes in the dependence of τ_{TN} on R_{TN} .

4 DISCUSSIONS AND FURTHER APPLICATIONS

It is necessary to check whether intrinsic AGN variability can provide quite different variability timescales in different epochs. Here, based on the 13years-long light curve $L_{bol, t, N5548}$, 100 different 2000days-long (about 10times of the intrinsic variability timescale 200days) light curves can be randomly collected from $L_{bol, t, N5548}$ with time duration from a randomly given starting time $0 < t_0/days < 3600$ to $t_0 + 2000$. The kbs09 method is applied to determine the variability timescales τ_d of the 100 different 2000days-long light curves. Then, we can find that the ratios of τ_d to the variability timescale 219days of $L_{bol, t, N5548}$ have mean value 1.02 with standard deviation 0.11. It is clear that light curves in different epochs cannot lead variability timescale varying so large as the results shown in Fig. 3 with large TDEs contributions. Similar results can be found from the mock light curves of $L_{bol, t, AGN}$ and $L_{bol, t, CAR}$.

Furthermore, there are seven more points we should note. First, in order to find more clearer effects of TDEs contributions on long-term AGN variability, the time duration is longer as 13years in the $L_{bol, t}$. Once there were shorter time durations applied, the dependence of τ_{TN} on R_{TN} would have larger scatters, due to probably only part of TDEs contributions covered in $L_{bol, t}$. Moreover, the simulating light curves are based on BH masses smaller than $10^8 M_{\odot}$. When BH mass is larger than $10^8 M_{\odot}$, more massive but shorter-lived main-sequence stars are necessary to simulate suitable TDEs, otherwise tidal disruption radius should be smaller than event horizon of central BH. Therefore, the large BH mass is selected to be $5 \times 10^7 M_{\odot}$ in the manuscript.

Second, as the discussed and shown results in MacLeod et al. (2010); Kelly, Bechtold & Siemiginowska (2009), the parameter σ and τ are probably connected. However, the connection between σ and τ is quite loose. Therefore, in the manuscript, there are no

considerations of the connection σ and τ , when the third kind of mock light curves $L_{bol, t}$ are simulated. With the similar considerations, due to the loose dependence of energy transfer efficiency and BH mass discussed in Davis & Laor (2011), the energy transfer efficiency η is randomly selected to be 0.06, 0.15 and 0.3. Otherwise, the expected energy transfer efficiency around $M_{BH} = 10^6 M_{\odot}$ should be small to be 0.008, an extremely smaller value.

Third, besides BH masses and intrinsic variability timescales, there are no further considerations on the other parameters related to TDEs model. Actually, the parameters, such as the stellar mass M_{\star} and impact parameter β , should have effects on the τ_{TN} , because commonly larger M_{\star} and β can commonly lead to stronger TDEs expected bolometric luminosities. As examples, Fig. 9 shows the dependence of τ_{TN} on the stellar mass M_{\star} and on the impact parameter β for the simulated light curves $L_{bol, t}$ by $L_{bol, t, N5548}$ plus TDEs contributions. For the shown dependence of τ_{TN} on the stellar mass M_{\star} , there are positive correlations with Spearman rank correlation coefficients about 0.35 and 0.61 ($P_{null} < 10^{-15}$) for the results with $\gamma = 4/3$ and with $\gamma = 5/3$, respectively. And, for the shown dependence of τ_{TN} on the β , there are positive correlations with Spearman rank correlation coefficients about 0.76 and about 0.54 ($P_{null} < 10^{-15}$) for the results with $\gamma = 4/3$ and with $\gamma = 5/3$, respectively. Even for M_{\star} around one solar mass or β gently larger than 1, τ_{TN} can be well larger than 2. Certainly, for the cases with smaller BH masses, the positive correlations on M_{\star} and on β should be not so strong. However, not similar as the central BH masses and redshift of normal AGN which can be well estimated through spectroscopic features, the M_{\star} and β can not be previously measured. And the main objective is to provide clues to detect probable hidden TDEs in normal AGN. Probability of more massive main-sequence stars being tidally disrupted with larger β in TDEs in normal AGN is not the objective of the manuscript. If there was a more massive main-sequence star was tidally disrupted with larger β in a normal broad line AGN, it would be more preferred to detect the expected hidden TDEs. Therefore, in the manuscript, effects of the model parameters related to the theoretical TDEs model are not discussed.

Fourth, as discussed in Kozłowski (2017), shorter time baseline should lead to underestimated process parameter τ in DRW/CAR process. Considering the expected longer τ due to larger contributions from TDEs, intrinsic values of process parameter τ should be larger than the currently determined values for the created mock light curves. Therefore, combining with the input value of process parameter τ for $L_{bol, t, CAR}$, larger values of τ_{TN} could be expected, leading to more apparent dependence of τ_{TN} on R_{TN} to support our final conclusions. Meanwhile, accepted the criterion reported in Kozłowski (2017) that there are good estimations of process parameters for light curves with $\tau/t_{exp} < 0.1$ (similar to process parameter τ divided by time baseline), the determined parameters are not biased for the mock light curves created with $\tau_0 = 200days$ ($\tau/t_{exp} \sim 200days/13years \sim 0.04 < 0.1$). Therefore, even only considering the results based on $\tau_0 = 200days$, similar conclusions on effects of TDEs contributions can be given.

Fifth, the standard theoretical TDE model discussed in Guillochon & Ramirez-Ruiz (2013); Guillochon, Manukian & Ramirez-Ruiz (2014); Mockler, Guillochon & Ramirez-Ruiz (2019) is applied in the manuscript, leading to expected time-dependent decline $t^{-5/3}$ at late times. However, besides standard TDE model expected variability pattern, there are slow TDEs, such as the discussed results in Graham et al. (2017), probably leading to shallower decline closer to t^{-1} . The slow TDEs could lead to much longer time durations than standard TDEs. However, based on the discussed results

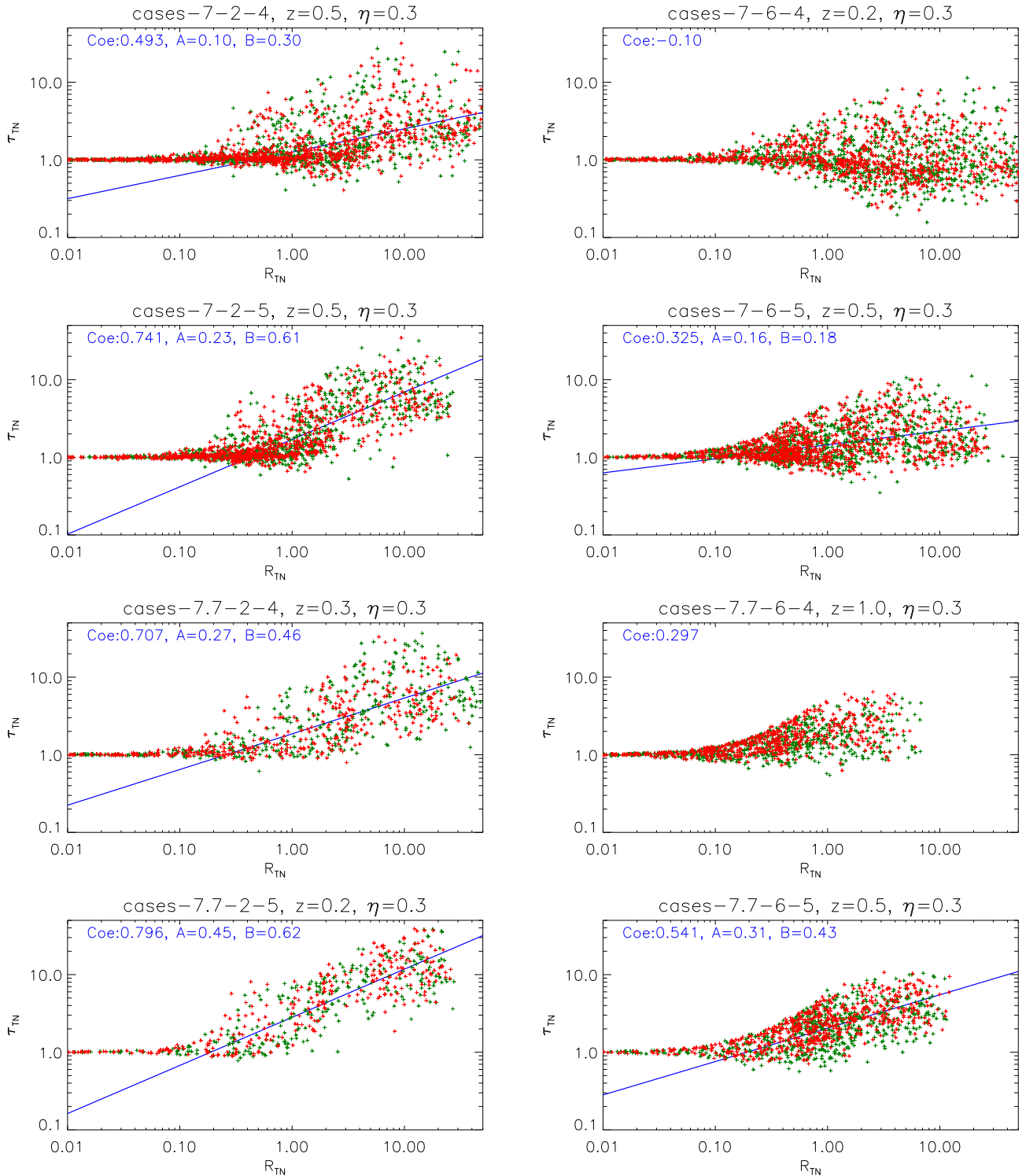


Figure 7. On the dependences of τ_{TN} on R_{TN} for the mock light curves based on the long-term variability $L_{bol, t, CAR}$. The results in the eight panels show the dependence with maximum Spearman Rank correlation coefficient among the 18 dependences in cases-7-2-4 (with $M_{BH} = 10^7 M_{\odot}$, $\tau_0 = 200days$ and $3 \times \gamma = 4$), cases-7-6-4 (with $M_{BH} = 10^7 M_{\odot}$, $\tau_0 = 600days$ and $3 \times \gamma = 4$), cases-7-2-5 (with $M_{BH} = 10^7 M_{\odot}$, $\tau_0 = 200days$ and $3 \times \gamma = 5$), cases-7-6-5 (with $M_{BH} = 10^7 M_{\odot}$, $\tau_0 = 600days$ and $3 \times \gamma = 5$), cases-7.7-2-4 (with $M_{BH} = 5 \times 10^7 M_{\odot}$, $\tau_0 = 200days$ and $3 \times \gamma = 4$), cases-7.7-6-4 (with $M_{BH} = 5 \times 10^7 M_{\odot}$, $\tau_0 = 600days$ and $3 \times \gamma = 4$), cases-7.7-2-5 (with $M_{BH} = 5 \times 10^7 M_{\odot}$, $\tau_0 = 200days$ and $3 \times \gamma = 5$), cases-7.7-6-5 (with $M_{BH} = 5 \times 10^7 M_{\odot}$, $\tau_0 = 600days$ and $3 \times \gamma = 5$) as the listed information in title of each panel. Meanwhile, the information of z and η are also listed in title of each panel. In each panel, Similar as the results shown in In each panel, pluses in red and in dark green show the results with SNR larger than 55 and smaller than 55, respectively. In each panel, due to large number of dense data points, the error bars with uncertainties about 20% - 25% are not plotted. In each panel, the calculated correlation coefficient (Coe) is marked in blue characters in top-left region for the correlation between τ_{TN} and R_{TN} ($R_{TN} > R_{cri}$). In each panel with correlation coefficient larger than 0.3, solid blue line shows the linear description $\log(\tau_{TN}) = A + B \log(R_{TN})$ to the correlation between τ_{TN} and R_{TN} ($R_{TN} > R_{cri}$) and the determined parameters of A and B are listed in blue characters in top-left region.

MNRAS **000**, 1–17 (2023)

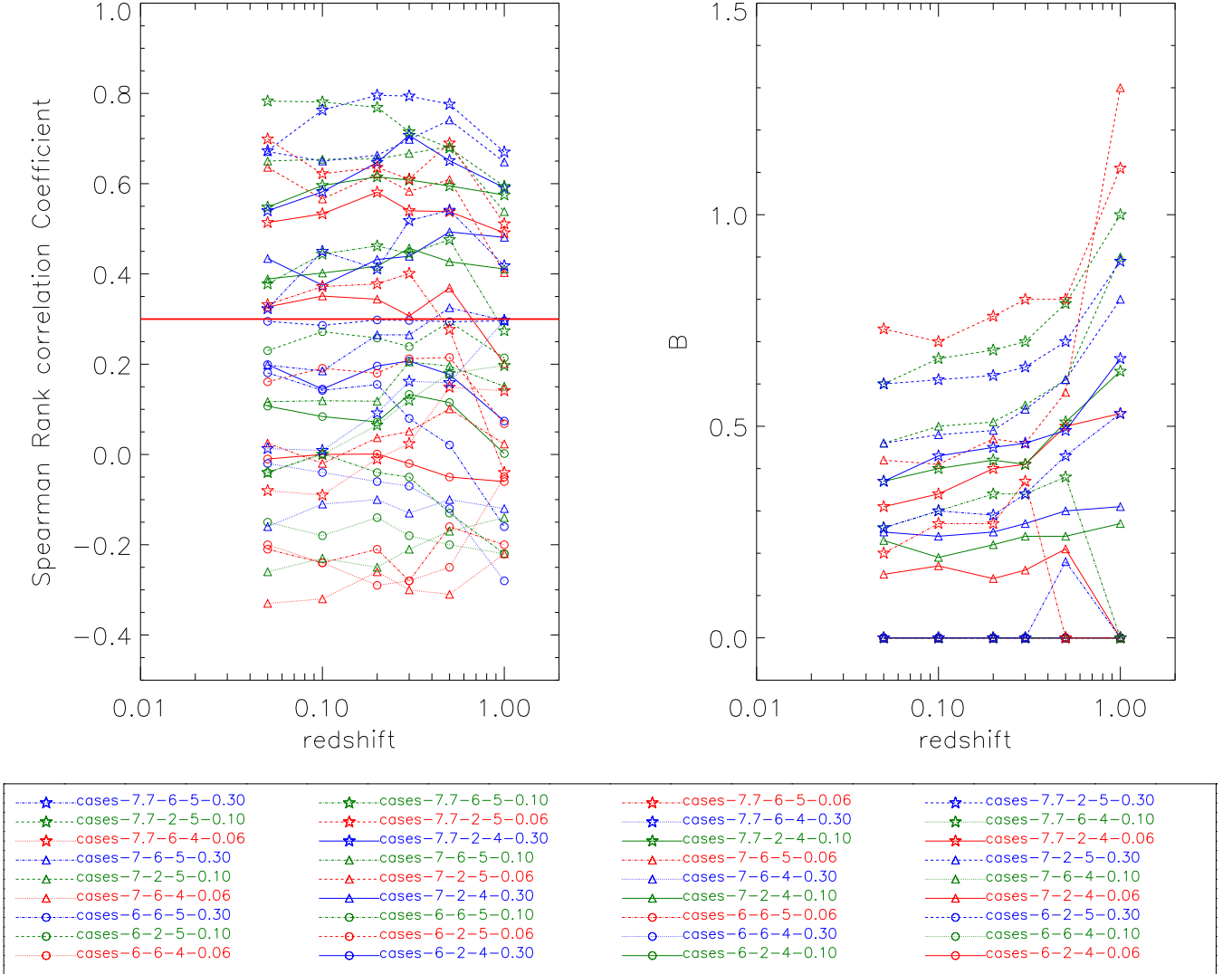


Figure 8. Top left panel shows properties of Spearman Rank Correlation Coefficients for all the dependences of τ_{TN} on R_{TN} for the cases with different M_{BH} , different τ_0 , different z , different γ and different η . Top right panel shows properties of B in the formula $\log(\tau_{TN}) = A + B \times \log(R_{TN})$ for all the dependences. Bottom panel shows the legends used in top panels. The four numbers included in 'cases-n0-n1-n2-n3' in legends have the following meanings, 'n0' means logarithmic BH mass, 'n1' means the value of $\tau_0/100$, 'n2' means the values of $3 \times \gamma$ and 'n3' means the value of η , for example, 'cases-7.7-2-4-0.30' means the 6 dependences (relative to six different values of redshift) of τ_{TN} on R_{TN} for the case with $M_{BH} = 5 \times 10^7 M_{\odot}$, $\tau_0 = 200$ days, $3 \times \gamma = 4/3$ and $\eta = 0.30$. In top right panel, due to many dependences with coefficients smaller than 0.3, there are some dependences with their B over-plotted with $B = 0$. In top left panel, horizontal red line marks the position of Spearman Rank correlation coefficient of 0.3.

above, more apparent difference between characteristic timescales of TDEs variability and characteristic timescales of intrinsic AGN variability should lead to more apparent dependence of τ_{TN} on R_{TN} . Therefore, even without considering rare numbers of slow TDEs, considerations of slow TDEs could lead to more apparent clues to support our final conclusions.

Sixth, as more recent discussions in Burke et al. (2022), host galaxy dilution could have strong effects on determined process parameter. However, accepted host galaxy contribution as an constant component with none variability (almost inevitable), the host galaxy dilution should have few effects on process parameter of τ , because the host galaxy contribution can be included in the parameter L_{b0} in Equation (12) above. In the manuscript, the ratio of τ from the

light curves with and without TDEs contributions are mainly considered, therefore, the host galaxy dilution has few effects on our final conclusions.

Seventh, although all the quasars with measurements of continuum luminosities are collected from Shen et al. (2011) to determine the dependence of bolometric luminosity on redshift shown in Fig. 1, some weak quasars are actually not included in the collected quasars, due to their lower continuum emissions. However, considering the very loose (or very weakly positive) dependence of DRW process parameter τ on luminosity as simply discussed in Kelly, Bechtold & Siemiginowska (2009); MacLeod et al. (2010), lower bolometric luminosities should lead to no variations of (or lower) DRW process parameter τ of intrinsic AGN variability. There-

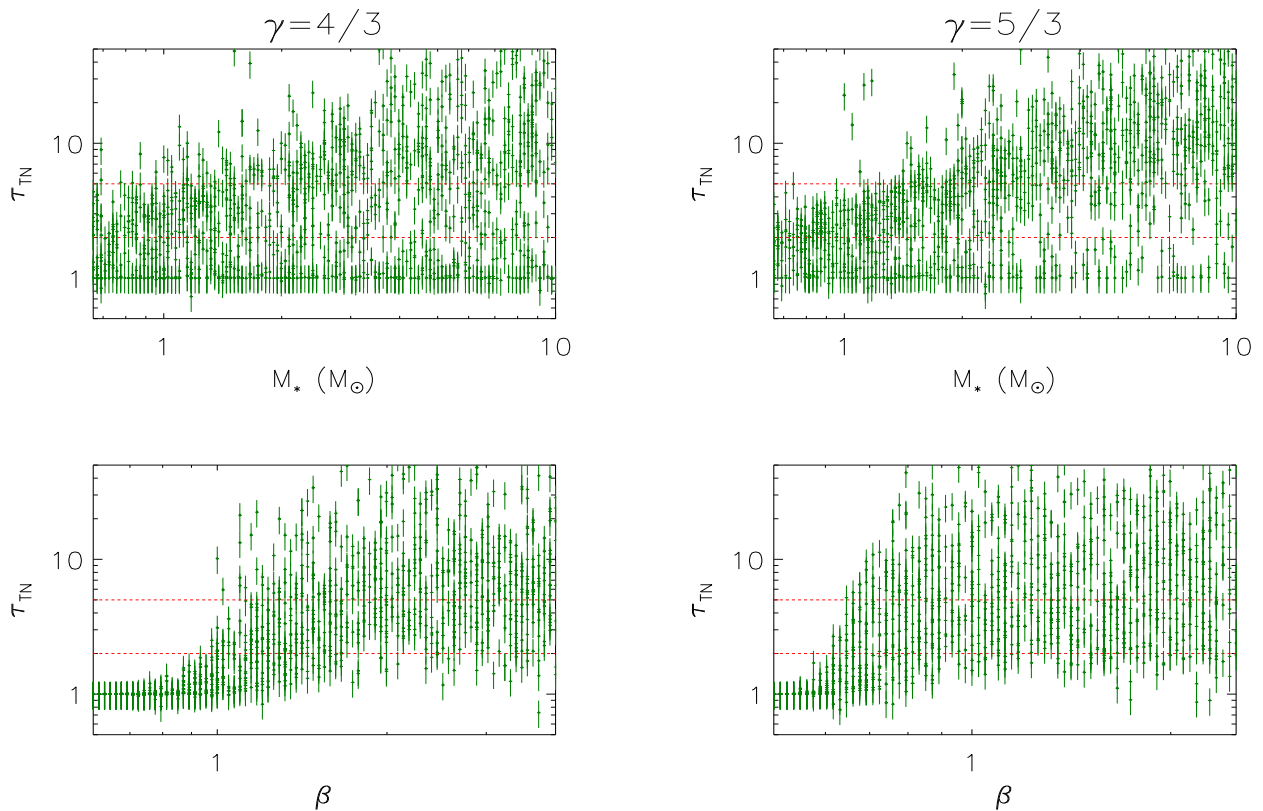


Figure 9. Dependence of τ_{TN} on the stellar mass M_* (top panels) and on the impact parameter β (bottom panels) for the simulated light curves $L_{\text{bol}, t}$ by $L_{\text{bol}, t, \text{N5548}}$ plus TDEs contributions with $\gamma = 4/3$ (left panels) and with $\gamma = 5/3$ (right panels). In each panel, horizontal dashed red lines show $\tau_{TN} = 2$ and $\tau_{TN} = 5$, respectively.

fore, even considering contributions of the lost weak quasars, there should be not different conclusions if accepted no dependence of DRW process parameter τ on luminosity, or lead to more apparent clues to support our final conclusions if accepted weakly positive dependence of DRW process parameter τ on luminosity.

Based on the expected effects of TDEs contributions on long-term AGN variability, to check variability properties in different epochs of normal AGN could provide clues on probable central hidden TDEs in normal AGN with apparently intrinsic variability. In one word, the results in the manuscript provide an interesting and practical method to detect probable hidden TDEs in normal AGN with apparent intrinsic variability, especially for AGN with smaller intrinsic variability timescales but BH masses larger than $10^7 M_\odot$. To report detected hidden TDEs in normal AGN through quite different τ in different epochs can provide robust evidence to support the results in the manuscript. Considering TDEs expected time durations about several years for $M_{\text{BH}} \sim 10^7 M_\odot$, baseline about (more than) 10years-long should be necessary for light curves to detected clues for hidden TDEs in broad line AGN. Therefore, combining light curves from different sky survey projects should be the efficient way to build light curves with baseline longer than 10 years. Unfortunately, there are quite different qualities, such as different baseline, different time steps, different SNRs, different covered wavelength ranges, different transmission curves for different filters, etc., for light curves from different sky survey projects. Before checking probably different intrinsic variability properties in different epochs from different sky survey projects, effects of the quite different qualities should be firstly

and clearly determined. In current stage, long-term light curves from CSS and from ZTF for a large sample of SDSS quasars have been collected, and basic results are currently in writing. In the near future, effects of different qualities on variability properties for light curves from CSS and ZTF and a small sample of quasars with quite different τ in light curves from CSS and from ZTF will be discussed and reported as soon as possible. It is a great pity that we can not currently give a clear estimation on detection rates of hidden TDEs through combinations of light curves from different sky survey projects, especially because we do not know what key parameters related to AGN dominate probable TDEs contributions. However, the results in the manuscript are showing a practicable way to detect hidden AGN in normal broad line AGN with apparent variability. To detect hidden TDEs in broad line AGN through different variability properties in different epochs is our main objective in the near future.

5 CONCLUSIONS

Finally, we give our main conclusions as follows. Based on the AGN variability templates simulated by the CAR process and the variability from theoretical TDEs model, effects of TDEs contributions can be well estimated on the long-term variability properties of normal AGN with apparent intrinsic variability. Stronger TDEs contributions can lead to longer variability timescale τ of observational long-term AGN variability, especially for AGN with smaller intrinsic variability timescales and with BH masses larger than $10^7 M_\odot$. Therefore, the re-

Table 2. Parameters B and Spearman rank correlation coefficients for the dependence of τ_{TN} on R_{TN}

τ_0	η	z	$M_6 = 1$ $B (\alpha)$	$M_6 = 10$ $B (\alpha)$	$M_6 = 50$ $B (\alpha)$	τ_0	η	z	$M_6 = 1$ $B (\alpha)$	$M_6 = 10$ $B (\alpha)$	$M_6 = 50$ $B (\alpha)$
$\gamma = 4/3$											
200	0.06	0.05	0 (-0.01)	0.15 (0.327)	0.31 (0.514)	600	0.06	0.05	0 (-0.20)	0 (-0.33)	0 (-0.08)
200	0.06	0.1	0 (-0.00)	0.17 (0.351)	0.34 (0.533)	600	0.06	0.1	0 (-0.24)	0 (-0.32)	0 (-0.09)
200	0.06	0.2	0 (0.001)	0.14 (0.344)	0.40 (0.581)	600	0.06	0.2	0 (-0.29)	0 (-0.26)	0 (-0.01)
200	0.06	0.3	0 (-0.02)	0.16 (0.307)	0.41 (0.540)	600	0.06	0.3	0 (-0.28)	0 (-0.30)	0 (0.024)
200	0.06	0.5	0 (-0.05)	0.21 (0.369)	0.50 (0.538)	600	0.06	0.5	0 (-0.25)	0 (-0.31)	0 (0.149)
200	0.06	1.0	0 (-0.06)	0 (0.201)	0.53 (0.491)	600	0.06	1.0	0 (-0.05)	0 (-0.22)	0 (0.141)
200	0.15	0.05	0 (0.107)	0.23 (0.389)	0.37 (0.548)	600	0.15	0.05	0 (-0.15)	0 (-0.26)	0 (-0.04)
200	0.15	0.1	0 (0.084)	0.19 (0.402)	0.40 (0.596)	600	0.15	0.1	0 (-0.18)	0 (-0.23)	0 (-0.00)
200	0.15	0.2	0 (0.072)	0.22 (0.417)	0.42 (0.615)	600	0.15	0.2	0 (-0.14)	0 (-0.25)	0 (0.065)
200	0.15	0.3	0 (0.133)	0.24 (0.457)	0.41 (0.608)	600	0.15	0.3	0 (-0.18)	0 (-0.21)	0 (0.120)
200	0.15	0.5	0 (0.115)	0.24 (0.427)	0.51 (0.595)	600	0.15	0.5	0 (-0.20)	0 (-0.17)	0 (0.180)
200	0.15	1.0	0 (0.002)	0.27 (0.411)	0.63 (0.575)	600	0.15	1.0	0 (-0.22)	0 (-0.14)	0 (0.197)
200	0.3	0.05	0 (0.199)	0.25 (0.434)	0.37 (0.540)	600	0.3	0.05	0 (-0.02)	0 (-0.16)	0 (0.013)
200	0.3	0.1	0 (0.145)	0.24 (0.375)	0.43 (0.582)	600	0.3	0.1	0 (-0.04)	0 (-0.11)	0 (0.009)
200	0.3	0.2	0 (0.196)	0.25 (0.432)	0.45 (0.647)	600	0.3	0.2	0 (-0.06)	0 (-0.10)	0 (0.092)
200	0.3	0.3	0 (0.207)	0.27 (0.439)	0.46 (0.707)	600	0.3	0.3	0 (-0.07)	0 (-0.13)	0 (0.162)
200	0.3	0.5	0 (0.177)	0.30 (0.493)	0.49 (0.651)	600	0.3	0.5	0 (-0.12)	0 (-0.10)	0 (0.159)
200	0.3	1.0	0 (0.074)	0.31 (0.481)	0.66 (0.591)	600	0.3	1.0	0 (-0.28)	0 (-0.12)	0 (0.297)
$\gamma = 5/3$											
200	0.06	0.05	0 (0.161)	0.42 (0.636)	0.73 (0.699)	600	0.06	0.05	0 (-0.21)	0 (0.025)	0.20 (0.332)
200	0.06	0.1	0 (0.191)	0.41 (0.566)	0.70 (0.622)	600	0.06	0.1	0 (-0.24)	0 (-0.02)	0.27 (0.372)
200	0.06	0.2	0 (0.180)	0.47 (0.621)	0.76 (0.636)	600	0.06	0.2	0 (-0.21)	0 (0.037)	0.27 (0.378)
200	0.06	0.3	0 (0.212)	0.46 (0.583)	0.80 (0.610)	600	0.06	0.3	0 (-0.28)	0 (0.051)	0.37 (0.401)
200	0.06	0.5	0 (0.215)	0.58 (0.609)	0.80 (0.690)	600	0.06	0.5	0 (-0.16)	0 (0.101)	0 (0.277)
200	0.06	1.0	0 (0.068)	1.30 (0.403)	1.11 (0.511)	600	0.06	1.0	0 (-0.20)	0 (0.023)	0 (-0.04)
200	0.15	0.05	0 (0.230)	0.46 (0.650)	0.60 (0.783)	600	0.15	0.05	0 (-0.04)	0 (0.117)	0.26 (0.378)
200	0.15	0.1	0 (0.272)	0.50 (0.654)	0.66 (0.781)	600	0.15	0.1	0 (0.002)	0 (0.119)	0.30 (0.444)
200	0.15	0.2	0 (0.258)	0.51 (0.655)	0.68 (0.769)	600	0.15	0.2	0 (-0.04)	0 (0.118)	0.34 (0.462)
200	0.15	0.3	0 (0.239)	0.55 (0.667)	0.70 (0.715)	600	0.15	0.3	0 (-0.05)	0 (0.205)	0.34 (0.445)
200	0.15	0.5	0 (0.294)	0.61 (0.682)	0.79 (0.679)	600	0.15	0.5	0 (-0.13)	0 (0.196)	0.38 (0.476)
200	0.15	1.0	0 (0.214)	0.90 (0.538)	1.00 (0.594)	600	0.15	1.0	0 (-0.22)	0 (0.151)	0 (0.274)
200	0.3	0.05	0 (0.295)	0.46 (0.671)	0.60 (0.673)	600	0.3	0.05	0 (0.181)	0 (0.198)	0.26 (0.323)
200	0.3	0.1	0 (0.286)	0.48 (0.650)	0.61 (0.763)	600	0.3	0.1	0 (0.142)	0 (0.185)	0.30 (0.450)
200	0.3	0.2	0 (0.298)	0.49 (0.663)	0.62 (0.796)	600	0.3	0.2	0 (0.155)	0 (0.265)	0.29 (0.411)
200	0.3	0.3	0 (0.297)	0.54 (0.698)	0.64 (0.794)	600	0.3	0.3	0 (0.080)	0 (0.265)	0.34 (0.518)
200	0.3	0.5	0 (0.294)	0.61 (0.741)	0.70 (0.776)	600	0.3	0.5	0 (0.021)	0.18 (0.325)	0.43 (0.541)
200	0.3	1.0	0 (0.296)	0.80 (0.648)	0.89 (0.670)	600	0.3	1.0	0 (-0.16)	0 (0.297)	0.53 (0.418)

1: From column 4 to column 6 and from column 10 to column 12, there are two numbers ' $B (\alpha)$ ' in each cell, where B is the slope of the formula $\log(\tau_{TN}) = A + B \times \log(R_{TN})$, and α is the determined Spearman rank correlation coefficient for the data points with R_{TN} larger than the critical values shown in textbody. If α is smaller than 0.3, then B is set to be zero.

2: M_6 means the BH mass in unit of $10^6 M_\odot$.

3: τ_0 means the input variability timescale in unit of days, when the third kind of $L_{bol, t}$ are simulated.

sults provide an interesting forward-looking and practicable method to detect central hidden TDEs in normal broad line AGN based on quite different variability properties in different epochs, especially in broad line AGN with shorter intrinsic variability timescales and with BH masses larger than $10^7 M_\odot$.

ACKNOWLEDGEMENTS

Zhang gratefully acknowledges the anonymous referee for giving us constructive comments and suggestions to greatly improve our paper. Zhang gratefully acknowledges the kind support from the Chinese grant NSFC-12173020 and NSFC-12373014. The paper has made use of the code of TDEFIT <https://tde.space/tdefit/> which is a piece of open-source software written by James Guillochon for the purposes of model-fitting photometric light

curves of tidal disruption events, and also made use of the code of MOSFIT (Modular Open Source Fitter for Transients) <https://mosfit.readthedocs.io/> which is a Python 2.7/3.x package for fitting, sharing, and estimating the parameters of transients via user-contributed transient models. The paper has made use of the data of NGC 5548 from AGNWATCH project (<https://www.asc.ohio-state.edu/astronomy/agnwatch/>) which is a consortium of astronomers who have studied the inner structure of AGN through continuum and emission-line variability. The paper has made use of the public code of FITEXY from the IDL Astronomy User's Library (<https://idlastro.gsfc.nasa.gov/ftp/pro/math/>). The paper has made use of the MCMC code <https://emcee.readthedocs.io/en/stable/index.html>, and made use of the MPFIT package <https://pages.physics.wisc.edu/~craigm/idl/cmpfit.html>.

DATA AVAILABILITY

The data underlying this article will be shared on reasonable request to the corresponding author (xgzhang@gxu.edu.cn).

REFERENCES

- Anderson, M.; Mooley, K.; Hallinan, G.; et al., 2020, *ApJ*, 903, 116 – 127
 Andrae R.; Kim, D. W.; Bailer-Jones C. A. L., 2013, *A&A*, 554, 137
 Bailer-Jones C. A. L., 2012, *A&A*, 546, A89
 Baldassare, V. F.; Geha, M.; Greene, J., 2020, *ApJ*, 896, 10
 Bentz, M. C.; Walsh, J. L.; Barth, A. J., et al., 2010, *ApJ*, 716, 993
 Blagorodnova, N.; Gezari, S.; Hung, T.; et al., 2017, *ApJ*, 844, 46
 Blanchard, P. K.; Nicholl, M.; Berger, E., et al., 2017, *ApJ*, 843, 106
 Bonnerot, C.; Rossi, E. M.; Lodato, G.; Price, D. J., 2016, *MNRAS*, 455, 2253
 Brockwell, P. J.; Davis, R. A. 2002, *Introduction to Time Series and Forecasting* (2nd ed.; New York: Springer)
 Burke, C. J.; Shen, Y.; Chen, Y.; Scaringi, S.; Faucher-Giguere, C.; Liu, X.; Yang, Q., 2020, *ApJ*, 899, 136
 Burke, C. J.; Shen, Y.; Blaes, O., et al., 2021, *Sci*, 373, 789
 Burke, C. J.; Liu, X.; Shen, Y.; et al., 2022, *MNRAS*, 516, 2736
 Cenko S. B.; Krimm, H. A.; Horesh, A.; et al., 2012, *ApJ*, 753, 77
 Chan, C.-H.; Piran, T.; Krolik, J. H.; Saban, D., 2019, *ApJ*, 881, 113
 Chan, C.-H.; Piran, T.; Krolik, J. H., 2020, *ApJ*, 903, 17
 Chen, J.; Dou, L.; Shen, R., 2022, *ApJ*, 928, 63
 Chornock, R.; Berger, E.; Gezari, S.; et al., 2014, *ApJ*, 780, 44
 Davis, S. W.; Laor, A., 2011, *ApJ*, 728, 98
 Dexter, J.; Begelman, M. C., 2019, *MNRAS Letter*, 483, 17
 Drake, A. J.; Djorgovski, S. G.; Mahabal, A.; et al., 2009, *ApJ*, 696, 870
 Drake, A. J.; Djorgovski, S. G.; Mahabal, A.; et al., 2011, *ApJ*, 735, 106
 Duras, F.; Bongiorno, A.; Ricci, F.; et al., 2020, *A&A*, 636, 73
 Favre P.; Courevoisier T. J. L.; Paltani S., 2005, *A&A*, 443, 451
 Foreman-Mackey, D.; Hogg, D. W.; Lang, D.; Goodman, J., 2013, *PASP*, 125, 306
 Gezari S.; Chornock, R.; Rest, A.; et al., 2012, *Nature*, 485, 217
 Gezari S., 2021, *ARA&A*, 59, 21
 Graham, M. J.; Djorgovski, S. G.; Drake, A. J.; Stern, D.; Mahabal, A. A.; Glikman, E.; Larson, S.; Christensen, E., 2017, *MNRAS*, 470, 4112
 Gromadzki, M.; Hamanowicz, A.; Wyrzykowski, L.; et al., 2019, *A&A*, 622, 2
 Guillochon, J.; & Ramirez-Ruiz, E., 2013, *ApJ*, 767, 25
 Guillochon, J.; Manukian, H.; Ramirez-Ruiz, E., 2014, *ApJ*, 783, 23
 Guillochon, J.; Nicholl, M.; Villar, A., et al., 2018, *ApJS*, 236, 6
 Guo, H.; Wang, J.; Cai, Z.; Sun, M., 2017, *ApJ*, 847, 132
 Hawkins, M. R. S., 2002, *MNRAS*, 329, 76
 Hayasaki, K.; Stone, N.; Loeb, A., 2016, *MNRAS*, 461, 3760
 Hinkle, J. T.; Holoien, T. W. -S.; Auchettl, K.; et al., 2021, *MNRAS*, 500, 1673
 Holoien, T. W.; Prieto, J. L.; Bersier, D.; et al., 2014, *MNRAS*, 445, 3263
 Holoien, T. W. S.; Kochanek, C. S.; Prieto, J. L.; et al., 2016, *MNRAS*, 455, 2918
 Holoien, T. W. S.; Huber, M. E.; Shappee, B. J.; et al., 2019, *ApJ*, 880, 120
 Horne, K.; De Rosa, G.; Peterson, B. M., et al., 2021, *ApJ*, 907, 76
 Hung, T.; Foley, R. J.; Ramirez-Ruiz, E.; et al., 2020, *ApJ*, 903, 31
 Kasliwal, V. P.; Vogeley, M. S.; Richards, G. T., 2015, *MNRAS*, 451, 4328
 Kathirgamaraju, A.; Barniol Duran, R.; Giannios, D., et al., 2017, *MNRAS*, 469, 314
 Kelly B. C.; Bechtold J.; Siemiginowska A., 2009, *ApJ*, 698, 895
 Kelly, B. C.; Becker, A. C.; Sobolewska, M.; Siemiginowska, A.; Uttley, P., 2014, *ApJ*, 788, 33
 Kochanek, C. S., 1994, *ApJ*, 422, 508
 Komossa, S.; Halpern, J.; Scharrel, N.; Hasinger, G.; Santos-Lleo, M.; Predehl, P., 2004, *ApJ Letter*, 603, 17
 Komossa, S., 2015, *JHEAp*, 7, 148
 Kozłowski, S.; Kochanek, C. S.; Udalski, A.; et al., 2010, *ApJ*, 708, 927
 Kozłowski, S., 2017, *A&A*, 597, 128
 Lee, C. H.; Hung, T.; Matheson, T.; et al., 2020, *ApJL*, 892, 1
 Li, S. L.; Cao, X. W., 2008, *MNRAS Letter*, 387, 41
 Leloudas, G.; Fraser, M.; Stone, N. C., et al., 2016, *Natur Astronomy*, 1, 2
 Liu, F. K.; Zhou, Z. Q.; Cao, R.; Ho, L. C.; Komossa, S., 2017, *MNRAS Letter*, 472, 99
 Liu, Z.; Li, D.; Liu, H.-Y., et al., 2020, *ApJ*, 894, 93
 Lodato, G.; King A. R.; Pringle J. E., 2009, *MNRAS*, 392, 332
 Loeb, A.; Ulmer, A., 1997, *ApJ*, 489, 573
 Lodato, G.; Franchini, A.; Bonnerot, C.; Rossi E. M., 2015, *JHEAp*, 7, 158
 Lu, K.; Du, P.; Hu, C., et al., 2016, *ApJ*, 827, 118
 Lynch, E. M.; Ogilvie, G. I., 2021, *MNRAS*, 501, 5500
 MacLeod C. L.; Ivezic, Z.; Kochanek, C. S.; et al., 2010, *ApJ*, 721, 1014
 Madejski, G.; Sikora, M., 2016, *ARA&A*, 54, 725
 Markwardt, C. B., 2009, *Astronomical Data Analysis Software and Systems XVIII ASP Conference Series*, Vol. 411, proceedings of the conference held 2-5 November 2008 at Hotel Loews Le Concorde, Quebec City, QC, Canada. Edited by David A. Bohlender, Daniel Durand, and Patrick Dowler. San Francisco: Astronomical Society of the Pacific, p.251
 Merloni, A.; Dwelly, T.; Salvato, A. G.; et al., 2015, *MNRAS*, 452, 69
 Mockler, B.; Guillochon, J.; Ramirez-Ruiz, E., 2019, *ApJ*, 872, 151
 Moreno, J.; Vogeley, M. S.; Richards, G. T.; Yu, W., 2019, *PASP*, 131, 3001
 Mushotzky, R. F.; Edelson, R.; Baumgartner, W.; Gandhi, P., 2011, *ApJL*, 743, 12
 Netzer, H., 2020, *MNRAS*, 488, 5185
 Panagiotou, C.; Papadakis, I.; Kara, E.; Kammoun, E.; Dovciak, M., 2022, *ApJ* accepted, arXiv:2207.04917
 Pancoast, A.; Brewer, B. J.; Treu, T., et al., 2014, *MNRAS*, 445, 3073
 Parkinson, E. J.; Knigge, C.; Long, K. S., et al., 2020, *MNRAS*, 494, 4914
 Pechacek, T.; Goosmann, R. W.; Karas, V.; Czerny, B.; Dovciak M., 2013, *A&A*, 556, 77
 Peterson, N. M.; Berlind, P.; Bertram, R.; et al., 2002, *ApJ*, 581, 197
 Peterson, B. M.; Ferrarese, L.; Gilbert, K. M.; et al., 2004, *ApJ*, 613, 682
 Rees, M. J., 1984, *ARA&A*, 22, 471
 Rees, M. J., 1988, *Nature*, 333, 523
 Richards, G. T.; Lacy, M.; Storrie-Lombardi, L. J.; et al., 2006, *ApJS*, 166, 470
 Rumbaugh, N.; Shen, Yue; Morganson, E.; et al., 2018, *ApJ*, 854, 160
 Sanchez-Saez, P.; Lira, P.; Mejia-Restrepo, J., et al., 2018, *ApJ*, 864, 87
 Sartori, Lia F.; Schwawinski, Kevin; Trakhtenbrot, B., et al., 2018, *MNRAS Letter*, 476, 34
 Sazonov, S.; Gilfanov, M.; Medvedev, P.; et al., 2021, *MNRAS*, 508, 3820
 Sheng, X.; Ross, N.; Nicholl, M., 2022, *MNRAS*, 512, 5580
 Shen, Y.; Richards, G. T.; Strauss, M. A.; et al., 2011, *ApJS*, 194, 45
 Short, P.; Nicholl, M.; Lawrence, A.; Gomez, S.; et al., 2020, *MNRAS*, 498, 4119
 Simm, T.; Salvato, M.; Saglia, R.; et al., 2016, *A&A*, 585, 129
 Stein, R.; van Velzen, S.; Kowalski, M.; et al., 2021, *Nature Astronomy*, 5, 510
 Stone, N. C.; Kesden, M.; Chang, R. M.; van Velzen, S.; *General Relativity and Gravitation*, 2019, 51, 30, arXiv:1801.10180
 Stone, Z.; Shen, Y.; Burke, C. J., et al., 2022, *MNRAS*, 514, 164
 Suberlak, K. L.; Ivezic, Z.; MacLeod, C., 2021, *ApJ*, 907, 96
 Tachibana, Y.; Graham, M. J.; Kawai, N.; Djorgovski, S. G.; Drake, A. J.; Mahabal, A. A.; Stern, D., 2020, *ApJ*, 903, 54
 Takata, T.; Mukuta, Y.; Mizumoto, Y., 2018, *ApJ*, 869, 178
 Torricelli-Ciamponi, G.; Foellmi, C.; Courvoisier, T. J. L.; Paltani S., 2000, *A&A*, 358, 57
 Tout, C. A.; Pols, O.; Eggleton, P.; Han, Z., 1996, *MNRAS*, 281, 257
 Tremaine, S.; Gebhardt, K.; Bender, R., et al. 2002, *ApJ*, 574, 740
 Ulrich, M. H.; Maraschi, L.; Urry C. M., 1997, *ARA&A*, 35, 445
 van Velzen, S.; Farrar, G. R.; Gezari, S.; et al., 2011, *ApJ*, 741, 73
 van Velzen, S.; Gezari S.; Cenko, S. B.; et al., 2019, *ApJ*, 872, 198
 van Velzen, S.; Gezari, S.; Hammerstein, E.; et al., 2021, *ApJ*, 908, 4
 Wagner, S. J.; Witzel, A., 1995, *ARA&A*, 33, 163
 Wang, T.; Yan, L.; Dou, L., et al., 2018, *MNRAS*, 477, 2943
 Williams, P. R.; Pancoast, A.; Treu, T.; et al., 2020, *ApJ*, 902, 74
 Wyrzykowski, L.; Zieliński, M.; Kostrzewa-Rutkowska, Z.; et al., 2017, *MNRAS Letter*, 465, L114

- Yan, Z.; Xie, F., 2018, *ApJ*, 475, 1190
Zanazzi, J. J.; Ogilvie, G. I., 2020, *MNRAS*, 499, 5562
Zhang, W. J.; Shu, X. W.; Sheng, Z. F., et al., 2022, *A&A*, 660, 119
Zhang, X. G.; Feng L. L., 2017, *MNRAS*, 464, 2203
Zhang, X. G.; Zhang, Y., Cheng, P., et al., 2021a, *ApJ*, 922, 248
Zhang, X. G., 2021b, *MNRAS Letter*, 500, 57
Zhang, X. G., 2022, *ApJ*, 928, 182
Zhang, X. G., 2022b, *MNRAS Letter*, 516, 66, Arxiv:2208.05253
Zhang, X. G., 2022c, *MNRAS Letter*, 517, 71, Arxiv:2209.09037
Zhang, X. G., 2023, *ApJ* accepted, Arxiv:2309.00852
Zhou, Z. Q.; Liu, F. K.; Komossa, S., et al., 2021, *ApJ*, 907, 77
Zu, Y.; Kochanek, C. S.; Peterson, B. M., 2011, *ApJ*, 735, 80
Zu, Y.; Kochanek, C. S.; Kozłowski, S.; Udalski, A., 2013, *ApJ*, 765, 106